

Thermal history during Mesozoic extension and Tertiary uplift in the Cameros Basin, northern Spain

M. P. Mata,* A. M. Casas,† A. Canals,‡ A. Gil† and A. Pocovi†

*Dpto. Geología. Facultad de Ciencias del Mar, Universidad de Cádiz, Pol. Río San Pedro, Pto. Real, 11510 Cádiz, Spain

†Departamento de Ciencias de la Tierra, Universidad de Zaragoza, 50009 Zaragoza, Spain

‡Departament de Cristallografia, Mineralogia i Dipòsits Minerals, Universitat de Barcelona, 08028 Barcelona, Spain

ABSTRACT

Detailed structural cross-sections, analysis of extensional structures and palaeotemperatures obtained from primary fluid inclusions in quartz and calcite veins from the extensional Cameros Basin (N Spain) allow an interpretation of its thermal evolution and its geometric reconstruction to be constrained. The Cameros Basin underwent an extensional stage during the Late Jurassic to Early Cretaceous, with a maximum preserved thickness of Mesozoic deposits of about 9000 m. During the Tertiary, the basin was inverted, allowing a large part of the sedimentary sequence to be exposed. Extensional deformation in individual beds created N120E-striking tension gashes in the synrift sequence, parallel to the master normal faults limiting the basin and dipping perpendicular to bedding. The extensional strain calculated from tension gashes varies between 4 and 12%. The number and thickness of veins increases the lower their position in the stratigraphic section. Palaeotemperatures were obtained from samples along a stratigraphic section comprising a thickness of 4000 m synrift deposits. Homogenization temperatures range from 107 to 225 °C. Palaeothermometric data and geometric reconstruction give a geothermal gradient of 27–41 °C km⁻¹ during the extensional stage and allow an eroded section of at least 1500 m to be inferred. Low-grade metamorphic assemblages in lutitic rocks of the deepest part of the basin presently exposed at surface imply *P–T* conditions of 350–400 °C and less than 2 kbar, which implies a geothermal gradient of about 70 °C km⁻¹. Since the metamorphic thermal peak is dated at 100 Ma, the *P–T* path indicates a heating event during the late Albian, probably linked to the reaching of thermal equilibrium of the continental crust after extension. The results obtained support the hypothesis of a synclinal basin geometry, with vertical superposition of Lower Cretaceous sedimentary units rather than a model of laterally juxtaposed bodies onlapping the prerift sequence.

INTRODUCTION

Diagenetic and very low-grade metamorphic evolution, as well as fluid flow in sedimentary basins, are a subject of increasing interest. Several methods have been applied to the study of the thermal evolution of sedimentary basins, including illite crystallinity, mineral assemblages, fluid inclusions, maturity of organic matter and apatite fission

tracks (Naeser *et al.*, 1989; Allen & Allen, 1990; Merriman & Frey, 1999; Merriman & Peacor, 1999, and references therein). Difficulties arise in the study of the low-grade metamorphic evolution of basins from the scarcity and restriction in the application of geo-thermometers and geo-barometers since chemical or isotopic equilibrium is not always achieved (De Caritat *et al.*, 1993; Essene & Peacor, 1995, 1997). Consequently, comparative studies are necessary to calculate their *P–T* conditions and to reconstruct their evolution. The extent and timing of fluid flow during thermal evolution in low-grade environments is also controversial. Some studies provide evidence for kilometre-scale fluid flow within the basin (Etheridge

Correspondence: M. P. Mata (pilar.mata@uca.es), Dpto. Geología, Facultad de Ciencias del Mar, Universidad de Cádiz, Pol. Río San Pedro, Pto. Real. 11510-Cádiz, Spain.

et al., 1983; Wall & Etheridge, 1988), but others (Yardley & Bottrell, 1992; Cartwright *et al.*, 1994) demonstrate that fluid flow is limited to the formation of veins. Heat flow and thermal gradients in extensional sedimentary basins are controlled by the basin geometry, mechanisms of basin formation, the magnitude of extension, nature of rocks and fluid flow within the basin fill (Mackenzie, 1978; Royden *et al.*, 1980; Andrews-Speed *et al.*, 1984; Aoyagi & Asakawa, 1984; Ter Voorde & Bertotti, 1994).

Extensional veins contemporaneous with extension are common in many sedimentary basins (Arthaud *et al.*, 1977; Guiraud & Séguret, 1984) and associated with different rock types (mainly sandstones and limestones). Extensional veins are usually perpendicular to the minimum stress axis (σ_3), and parallel to normal faults and tensional joints (Arthaud & Séguret, 1972; Ramsay & Huber, 1983; Hancock, 1985; Angelier, 1994; Dunne & Hancock, 1994). Quartz and calcite crystals within veins are contemporary with extension. Fluid inclusions and isotope analysis provide one of the best tools available for determining properties of fluids associated with geological processes (Mullis, 1987; Burrus, 1989; Goldstein & Reynolds, 1994; Kirschner *et al.*, 1995; Sharp, 1999, and references therein) and can be considered as a time capsule storing information about ancient temperatures, pressures and fluids (Goldstein & Reynolds, 1994). Therefore, microthermometric studies of primary fluid inclusions from extensional veins can be used to understand diagenetic evolution (Burrus, 1989). Determination of palaeotemperatures and palaeogradients in ancient sedimentary basins is also an important tool to constrain basin models, concerning both their geometry and tectonic setting (Magara, 1976; Miall, 1984; Allen & Allen, 1990; Green *et al.*, 1995; Heydari, 1997; Willett *et al.*, 1997). In addition, the temperature that rocks passed through in a sedimentary basin is a decisive factor in controlling the process of hydrocarbon formation, both in the oil and the gas windows (Quigley & Mackenzie, 1988; Zhao *et al.*, 1996) and is essential for the evaluation and exploration of hydrocarbon potential.

The Cameros Basin is a particular area that underwent a complex tectonothermal evolution within the Mesozoic intraplate basins in the northern Iberian plate. Although its evolution remains controversial, it is believed that the evolution consisted of: (1) an important period of extension (Early Cretaceous) giving 8 km of synrift deposits; (2) an early compression without inversion, with folding and cleavage, at the end of the Early Cretaceous (Casas-Sainz & Gil-Imaz, 1998), and (3) low-grade metamorphism in the depocentre of the basin with a thermal peak dated about 100 Ma. (Goldberg *et al.*, 1988). The basin was completely inverted during the Tertiary (Casas-Sainz, 1993; Guimerà *et al.*, 1995; Casas-Sainz & Gil-Imaz, 1998), allowing a continuous stratigraphic section of the basin fill to be exposed at the surface. The geometry of the extensional Cameros Basin is subject to discussion with two main models being proposed: (i) vertical superposition of the present-day outcropping

sedimentary units, which implies that the sedimentary filling was 9 km thick (Casas-Sainz & Gil-Imaz, 1998) and (ii) lateral shingling of the sedimentary units, with a thickness of the synrift sequence not larger than 5 km (Guiraud & Séguret, 1984; Casas-Sainz, 1993; Guimerà *et al.*, 1995). The role of fluids has been also controversial: Casquet *et al.* (1992) proposed a clear relation between mineral assemblages and fluid circulation, whereas Mata (1997) and Mata *et al.* (1998) proposed a local overprinting caused by a retrograde hydrothermal event on a low-grade prograde sequence.

In this paper we use structural analysis, restored cross-sections, fluid inclusion data, stable isotopes and mineral assemblages to reconstruct the thermal history and geothermal gradients of the Cameros Basin during Cretaceous time. For this purpose, we use data from extensional gashes corresponding to the rifting stage, and mineralogical assemblages formed during the peak of the thermal event, corresponding to a later stage in its evolution. On the basis of the results, hypotheses for the geometry and the role of fluids in the Cameros Basin are revised.

GEOLOGICAL SETTING

The Iberian chain (Fig. 1) is an intraplate mountain range that occupies the central-eastern part of the Iberian peninsula (Julivert, 1978; Alvaro *et al.*, 1979; Capote, 1983). It consists of three main structural units:

1 A Variscan 'basement', formed by Cambrian to Carboniferous sedimentary sequences, mainly sandstones and shales, up to 10 km thick (Ferreiro *et al.*, 1991; Casas *et al.*, 2000). The Variscan structures are N-S to NW-SE and E-W folds, and north-verging thrusts. Late-Variscan fractures (Permian in age) show two main strikes: NW-SE and NE-SW. Variscan structures and late Variscan fracturing strongly conditioned the location and orientation of extensional and compressional structures during the Mesozoic and the Tertiary (Salas & Casas, 1993). The Palaeozoic is overlain by Lower and Middle Triassic sandstones and limestones.

2 The Middle-Upper Triassic, consisting of shales and gypsum, are the main detachment levels at the regional scale (Pyrenees and Iberian Chain), both for the extensional and the compressional deformation (Guimerà & Alvaro, 1990; Casas-Sainz & Gil-Imaz, 1998).

3 The Mesozoic (Jurassic-Cretaceous) and Tertiary (Eocene-Oligocene) sedimentary cover shows maximum thickness of more than 5 km at the eastern (Maestrat Basin) and western (Cameros Basin) sectors of the Iberian Chain. Its structure is defined by NW-SE, E-W and NE-SW folds and thrusts in the northern part of the chain, and changes to N-S in the south-westernmost sector (Muñoz-Martín & De Vicente, 1998).

The north-eastern part of the Iberian plate underwent two Mesozoic rifting stages (Early Triassic and Early Cretaceous), each followed by thermal subsidence

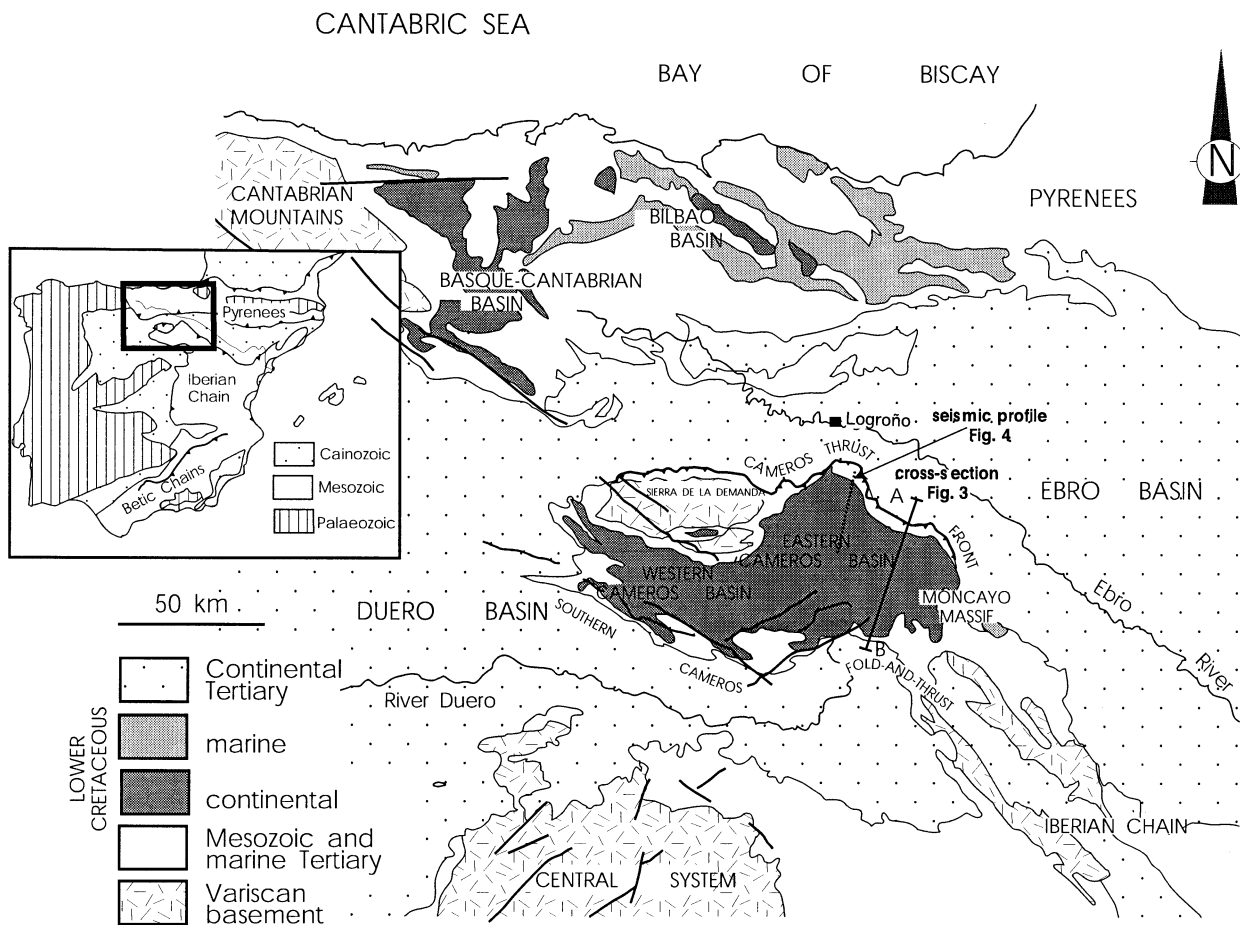


Fig. 1. Geological setting of the Eastern Cameros Basin and other Cretaceous basins within the northern Iberian peninsula. The locations of the cross-section and seismic reflection profile of Figs 3 and 4, respectively are also shown.

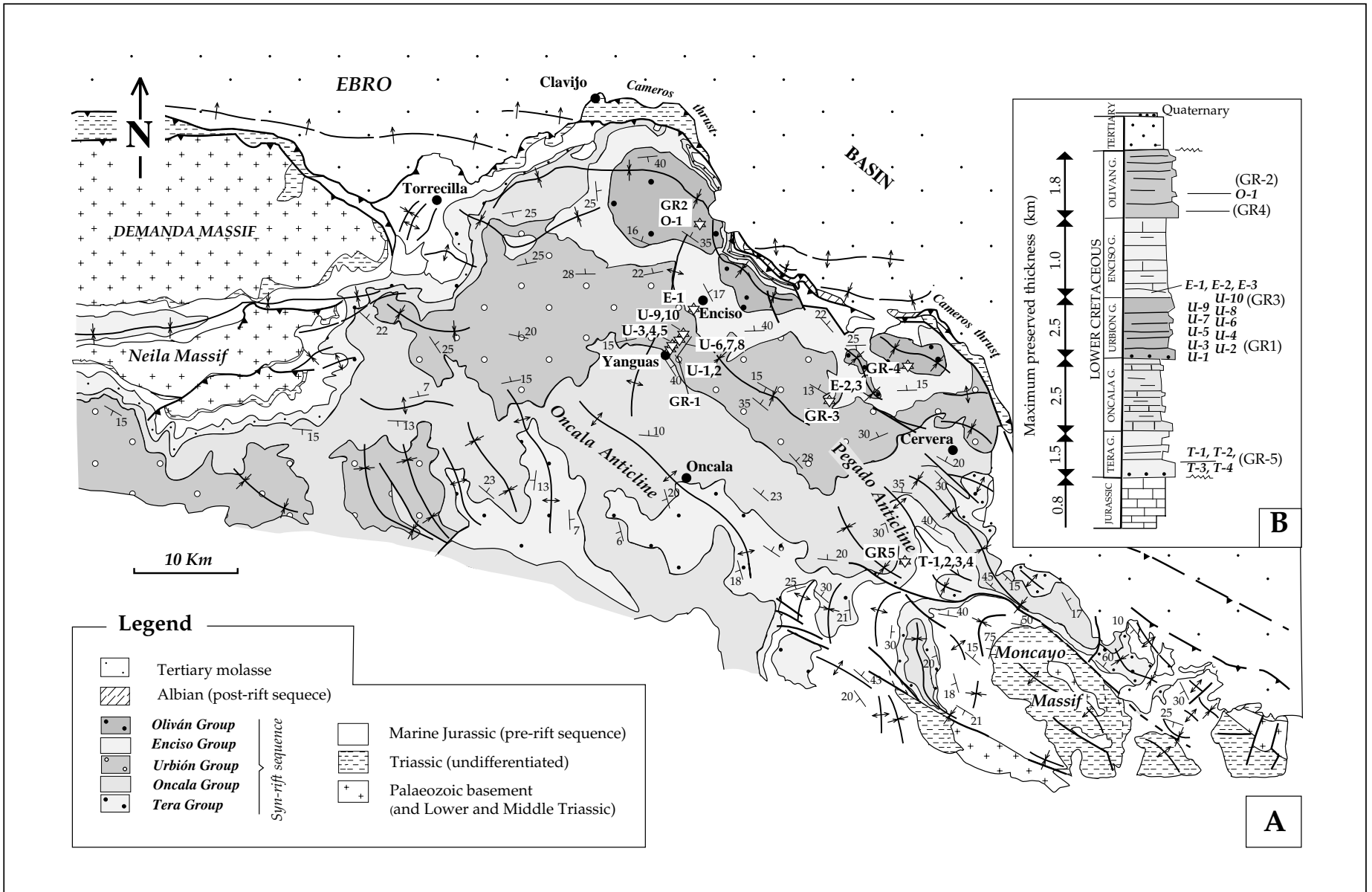
(Ferreiro *et al.*, 1991; Salas & Casas, 1993). Rifting was associated with extension in the western Tethys and the opening of the northern Atlantic (Ziegler, 1989). Triassic rifting produced sedimentary basins with sediment thicknesses of up to 1500 m (Sopeña *et al.*, 1983; Arche & López-Gómez, 1996). Extension was accomplished by faults probably transecting the whole crust, since magmatism of mantle origin (alkali basalts) is found in many places (Lago *et al.*, 1988; Pocovi *et al.*, 1997). Early Cretaceous rifting gave rise to important extensional basins, such as the Cameros and Maestrat basins where sediment thicknesses of more than 5 km accumulated (Mas *et al.*, 1993; Salas & Casas, 1993; Casas-Sainz & Gil-Imaz, 1998).

The Cameros Basin, now exposed in the Cameros Massif, forms the north-western most part of the Iberian Chain. It comprises up to 8 km of Upper Jurassic to Lower Cretaceous strata. It is interpreted to be a half graben with a northern active border composed of listric normal faults striking NW–SE to E–W. Synrift strata form a wedge that progressively thins toward the south-west and ends more abruptly toward the north-east (Guiraud, 1983; Casas-Sainz & Gil-Imaz, 1998).

Stratigraphy of the basin

The Cameros Massif can be divided into two sectors (Fig. 1) (Tischer, 1966; Salomon, 1980; Guiraud & Séguret, 1984; Mas *et al.*, 1993): (1) a western sector, where the thickness of terrestrial Upper Jurassic – Lower Cretaceous strata reaches more than 2 km, with large WNW-trending folds and thrusts, and (2) an eastern sector, where Mesozoic strata are 9 km thick and form gentle NW-trending folds (Fig. 2). We have centred our study in the eastern sector of the Cameros Massif where metamorphic minerals, a large number of veins, and the maximum thickness of synrift sediments occur.

The Mesozoic series of the Cameros Basin lies unconformably on Variscan basement, consisting of Precambrian shales and Cambro-Ordovician sandstones and shales, folded and thrust in an E–W direction. Lower and Middle Triassic strata reach a maximum thickness of 250 m and consist of terrestrial and shallow marine deposits. Upper Triassic strata consist of lutite and gypsum of variable thickness (0–500 m), and were the regional detachment level for the Mesozoic sedimentary cover, both during extension and compression



(Casas-Sainz, 1993; Casas-Sainz & Gil-Imaz, 1998). Marine Jurassic carbonate rocks, unconformably lying on the Triassic and the Palaeozoic (Goy *et al.*, 1976; Aurell *et al.*, 1992) range in thickness between 400 and 800 m. They consist of massive, laminated, and bioclastic limestones, and successions of alternating marl and limestone.

The Upper Jurassic – Lower Cretaceous synrift sequence, Kimmeridgian to Albian in age, is represented in the Eastern Cameros Massif by five lithostratigraphic groups (Tischer, 1966): Tera, Oncala, Urbión, Enciso and Oliván (Fig. 2), collectively termed 'Wealdian', with a maximum combined thickness of about 8 km. They consist of fluvial and lacustrine facies, with some brackish and lagoonal episodes, and show maximum individual preserved thickness of 1500, 2500, 2500, 1000 and 1800 m, respectively. The fluvial series (mainly represented in the Tera, Urbión and Oliván Groups) consist of quartzitic and arkosic sandstones, siltstones and shales derived from acidic sources (Mata *et al.*, 2000). The lacustrine episodes (dominant in the Oncala and Enciso Groups) are represented by silty and limestone beds. The post-rift sequence consists of upper Albian marine limestones 50 m thick (Muñoz *et al.*, 1997), upper Albian to Cenomanian sandstones (Utrillas Formation) with interbedded coal measures, and Upper Cretaceous marine limestones (not outcropping in the Eastern Cameros Massif, (Fig. 2).

Structure and Mesozoic–Tertiary evolution

The northern border of the Cameros Massif is an E–W-striking north-verging thrust, with a horizontal displacement of 25 km over the Tertiary molasse of the Ebro Basin. Its southern limit is defined by south-verging thrusts with horizontal displacements of 5 km (Guimerà *et al.*, 1995; Casas *et al.*, 2000).

The Eastern Cameros Massif shows an overall synclinal geometry, with its northern limb stratigraphically thinned (1:5) with respect to the southern limb (Figs 2 and 3). Dips in the southern limb vary between 10° and 35°N. The northern limb of the syncline shows dips up to 80°S, with an average value of 50°S (Casas-Sainz, 1993). Along the northern border of the Cameros Massif several normal faults, with throws ranging from centimetres to tens of kilometres can be recognized (Casas-Sainz & Gil-Imaz, 1998). These faults indicate that the present-day northern border of the Cameros Massif, resulting from thrusting during Tertiary inversion, records the shape of the northern margin of the Mesozoic Basin.

The structure of the Cameros Massif was controlled by Mesozoic extension, Early Cretaceous folding and

Tertiary folding and thrusting (Casas-Sainz & Gil-Imaz, 1998):

1 During the Late Jurassic – Early Cretaceous, crustal extension affected both the prerift and the synrift sequences. Extension in the prerift sequence (marine Jurassic) was achieved by normal faults, rooting in Upper Triassic, low-strength evaporites (Fig. 3). In the synrift sequence, extension was achieved both by normal syndimentary faulting linked to growth strata and by internal brittle deformation, mainly hydroplastic faults and tension gashes (Guiraud, 1983; Guiraud & Séguret, 1984; Diaz-Martínez, 1988; Mata *et al.*, 1996). A NNE–SSE to NE–SW extension direction is obtained from structural analysis of tension gashes and faults (Guiraud & Séguret, 1984). The isopachs of the synrift sedimentary units suggest a half-graben basin geometry (Guiraud & Séguret, 1984; Casas-Sainz, 1993; see Fig. 3). In a regional 3-D view, the normal faults marking the northward edge of the basin are interpreted to have a general NW–SE strike with some E–W segments (Casas-Sainz, 1993).

2 Cleavage and low-grade metamorphic assemblages in the Cameros Massif are a unique feature of the Iberian Chain and have been interpreted as the result of Cretaceous (Aptian to Albian) shortening and folding in an incipiently thinned continental crust (Casas-Sainz & Gil-Imaz, 1998). The mechanisms for cleavage formation are pressure solution in the calcareous rocks, and orientated recrystallization of phyllosilicates in lutites. The absolute dating of the thermal metamorphic peak by Ar³⁹–Ar⁴⁰ isotope analysis of illite (Goldberg *et al.*, 1988) and K–Ar analysis of illite (Casquet *et al.*, 1992) indicates an age ranging between 86 and 108 Ma. Preliminary estimations of *P–T* conditions (Guiraud & Séguret, 1984) indicate that maximum temperatures did not reach 450 °C, at less than 2 kbar. Textural relations show that chloritoid crystals are randomly orientated in a strongly orientated matrix and cut across the cleavage fabric (Casas-Sainz & Gil-Imaz, 1998). This textural relationship indicates, at the regional scale, that the metamorphic peak postdates both the extension stage and the cleavage-related folding.

3 The present-day geometry of the Cameros Basin (Fig. 3A) is mainly due to Tertiary contraction, which inverted and transported the basin 25 km northward (Guimerà & Alvaro, 1990; Casas-Sainz, 1993; Guimerà *et al.*, 1995; Casas-Sainz & Gil-Imaz, 1998). The main structure is a single, low-angle thrust incorporating slices of Variscan 'basement', cropping out in the Sierra de la Demanda (Figs 1 and 2). Tertiary compressional structures strike E–W to NW–SE. The footwall of the main thrust consists of up to 4 km of Tertiary molasse of the Ebro basin (Muñoz-Jiménez & Casas-Sainz, 1996)

Fig. 2. A. Geological sketch of the Eastern Cameros Massif showing the location of the samples used for palaeothermometric studies. B. Stratigraphic log of the Upper Jurassic to Lower Cretaceous Cameros Massif showing the stratigraphic location of the studied samples.

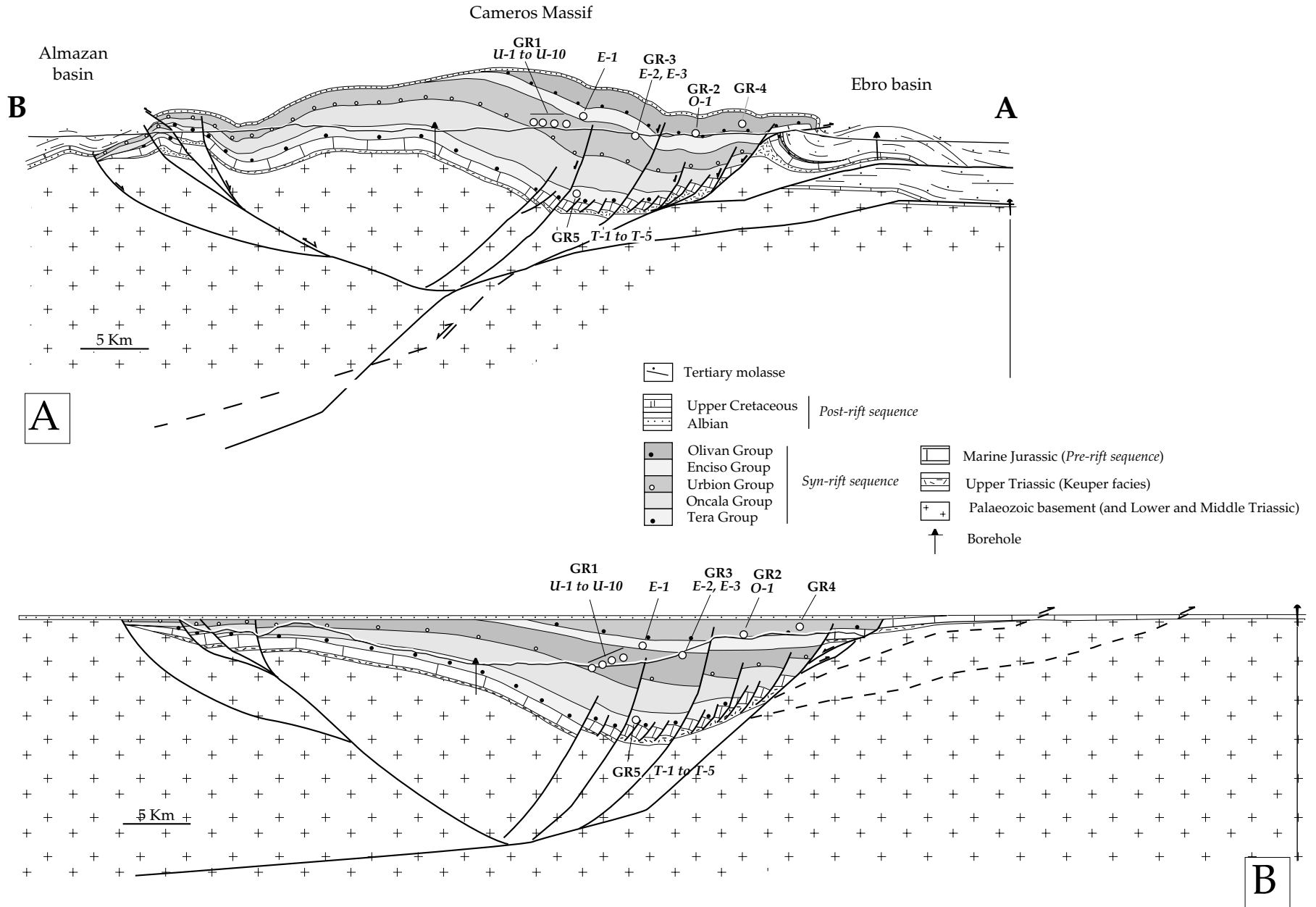


(Fig. 4), underlain by a Mesozoic succession that reaches a maximum thickness of 700 m (Lanaja, 1987). The southern border of the massif is formed by NW–NE-striking, south-verging thrusts with horizontal displacements of up to 5 km (Platt, 1990; Guimerà *et al.*, 1995; Casas *et al.*, 2000).

LOCATION OF OUTCROPS, SAMPLES AND METHODS

Structural measurements at five different sites (GR1, GR2, GR3, GR4 and GR5) and 18 samples were taken from the Urbión to the Oliván group in a continuous prograde sequence (Fig. 2 and Table 1) of the Eastern Cameros Basin. Samples were accurately located within the stratigraphic series, taking into account the thickness of the different sequences, obtained from direct measurement in the field (Guiraud, 1983; Guiraud & Séguret, 1984) and checked by the interpretation of seismic reflection profiles and borehole data (Casas-Sainz & Gil-Imaz, 1998) (Fig. 4). These data correspond to the maximum thickness preserved in the basin centre. Most samples were taken from quartz-rich veins, and the host rocks are mainly sandstones, siltstones and continental limestones. Host rock mineral assemblages range from deep diagenesis to epizone (Table 1). The methodology used includes structural analysis of the tension gashes, mineralogical and fluid inclusion studies and isotopic analysis.

Microthermometric analyses were performed on a Linkam THMS-600 heating–freezing stage calibrated using natural pure CO₂ inclusions, bidistilled water and Merck standards. Errors are ± 0.2 °C for freezing and ± 2 °C for heating. Raman and microprobe analysis of some of the veins have been carried out at SCT of Barcelona University. Scanning electron microscopic studies on polished thin sections were made in a Hitachi S-3200N, equipped with a Noran X-ray energy-dispersive system, and operated at 20 kV at the University of Michigan. Electronic Microprobe Analysis (EMPA) of host rock was performed on a Cameca Camebax SX 50 at the University of Granada. Operating conditions were 20 kV accelerating potential and 30 μ A beam current. Anhydrous oxides and simple silicates were used as probe standards. Isotopic data in this study were procured from 16 quartz and calcite vein samples. For oxygen isotope analysis of quartz, oxygen was extracted using the BrF₅ technique (Clayton & Mayeda, 1963). Carbon dioxide was extracted from carbonates using phosphoric acid (McRea, 1950). The isotopic ratios of the CO₂ and O₂ gases were measured using a Finnigan Mat 251 mass spectrometer. Isotopic compositions are reported in delta notation relative to VSMOW for oxygen

and VPDB for carbon. XRD analysis of host rock and veins were determined using a Phillips 1710, with CuK α radiation and automatic slit of the University of Zaragoza.

GEOMETRY OF EXTENSIONAL STRUCTURES

In the studied areas, tension gashes are arranged in sets and usually cross-cut whole strata. Their thickness ranges between 1 and 80 cm. The maximum thickness of veins is found at the base of the Urbión Group (samples U-1 to U-3) and at the Pégado anticline (T-1 to T-4). Both areas possibly correspond to the deepest zones within the basin, at the level of the present outcrop (Figs 2 and 3). Veins are filled with milky and fibrous quartz crystals in quartzitic sandstones, whereas calcite veins show a more massive infill in limestones.

Tension gashes are nearly perpendicular to bedding, both with horizontal or dipping beds (Fig. 5), except for site GR4, located on the western limb of the Pégado anticline, where they are at 60° to bedding (Fig. 5). The mean direction of tension gashes is N120E, which gives a NNE–SSW extension direction for the central part of the basin. The geometric relationship between bedding and tension gashes, and their mean direction, parallel to the main normal faults limiting the basin toward the north, indicates that they are contemporaneous with the rifting stage, and pre-date Tertiary folding. Where the relationship between tension gashes and cleavage can be seen (for example, at the limbs of the Pégado anticline, Fig. 2), cleavage post-dates extensional structures.

Although it is difficult to quantify the extensional deformation due to tension gashes, because of the very nature of brittle deformation, an attempt was made to measure the thickness of every extensional gash perpendicular to bedding in several outcrops. The cumulative length (i.e. cumulative vein thickness) was related with the initial length of the bed, giving the total deformation in each outcrop during extension (Fig. 5A). The amount of extension determined for individual strata is given by the relationship $(\sum E_g / \sum E_m) \times 100$, where E_g is the thickness of each tension gash and E_m the length of the nondeformed bed between two consecutive gashes. Their values range between 2% and 12% (Fig. 5A), with single important variations found between different strata. At the lower part of the Urbión Group (GR1, Fig. 5A) the amount of extension calculated for five strata show values of 4, 2, 12, 7 and 5%. In sites GR2 and GR3 the amount of extension varies between 7 and 10% and at the Pégado anticline it is 12%.

In some places tension gashes are associated with pinch-and-swell structures within sandstone strata, and bed-parallel cleavage in incompetent beds. The geometry

Fig. 3. A. Cross-section showing the present-day geometry of the eastern Cameros Massif. B. Restored cross-section at the end of the Late Cretaceous. Cross-section located in Fig. 1. The location of sample sites (projected along each stratigraphic level) is indicated.

Table 1. Descriptions of samples and analytical details of veins. qtz: quartz; kfs: potassium feldspar; pl: plagioclase; chl: chlorite; ill: illite; I/S: interlayer illite smectite; ab: albite; cal: calcite; prl: pyrophyllite; ms: muscovite; pg: paragonite; cld: chloritoid; py: pyrite; dol: dolomite.

| Host rock | | | Vein | | | | | | | |
|-----------|------------|-------------------------------|----------|------------|------|---|--|----------------|----------------|----------------------|
| Sample | Lithology | Mineralogy (XRD) | Width | Mineralogy | Type | $T_{mi}(\sigma, n^0)$ $T_{mcc}(\sigma, n^0)$ | $T_h(\sigma, n^0)$ $T_hCO_2(\sigma, n^0)$ | $\delta^{18}O$ | $\delta^{18}O$ | $\delta^{18}O(H_2O)$ |
| O-1 | Sandstone | qtz-kfs/pl-chl-ill-I/S | 1–2 cm | qtz | I | | 107 (17,16) | | | |
| E-3 | Sandstone | qtz-kfs/pl-chl-ill-I/S | ? | qtz | – | | | + 17.7 | | |
| E-2 | Sandstone | qtz-kfs-chl-ill-chl/sm-ab | ? | qtz-ab | – | | | + 16.8 | | |
| E-1 | Limestone | qtz-chl-ill-chl/sm-ab-cal | 2–3 cm | qtz-cal | I | – 4.9 (0.3, 19) | 160 (6,25) | + 24.3 | | 10‰ |
| U-10 | Sandstone | qtz-chl-ill-chl-ab-cal | 20 cm | qtz-cal | – | | | + 15.3 (cal) | – 9.1 | |
| U-9 | Sandstone | qtz-chl-ill-chl-prl-ms-pg-ca | 20 cm | qtz-cal | – | | | + 17.4 (qtz) | | |
| U-8 | Siltstone | qtz-chl-ms-pg | ? | qtz | | | | + 22.1 (cal) | – 8.2 | |
| U-7 | Sandstone | qtz-chl-ms-pg-cld | ? | qtz-cal | I | – 5.2 (0.1, 10) | 158 (6,18) | + 17.3 | | 2.5‰ |
| U-6 | Sandstone | qtz-chl-ms-pg-cld-py | 10 cm | qtz | – | | | + 22.1 (cal) | – 7.5 | |
| U-S | Sandstone | qtz-chl-ms-pg-cld | 10 cm | qtz | I | – 5.1 (0.4, 25) | 151 (20,12) | + 16.6 | | 1‰ |
| U-4 | Sandstone | qtz-chl-ms-pg-cld-(py) | 10–50 cm | qtz | I–II | – 4.8 (0.3, 49) 6.4 (1.3, 24) | 183 (15,64) | + 17.5 | | 4.5‰ |
| U-3 | Sandstone | qtz-chl-ms-pg-cld-py | 10–50 cm | qtz | I–II | – 2.8 (0.7, 15) | 197 (30,15) | | | |
| U-2 | Sandstone | qtz-chl-nis-pg-cld-py | 10–50 cm | qtz | II | – 5.1 (0.2, 15) 7.1 (0, 5, 7) | 199 (7,19) | + 19.2 | | 7.5‰ |
| U-1 | Sandstone | qtz-chl-ms-pg-cld-py | 10–50 cm | qtz | II | – 5.2 (0.5, 25) 7.4 (0.5, 20) | 208 (14,19) 22.1 (1.5, 9) | + 19.3 | | 8‰ |
| T-4 | Limestone | qtz-chl-ill-chl/sm-cal-dol | 60 cm | qtz | – | | | + 26.5 | | |
| T-3 | Siltstone | qtz-chl-ill-chl/sm-cal-dol | 80 cm | qtz-cal | I | – 6.7 (0.4, 14) | 223 (9, 19) | + 20.7 | | 10‰ |
| T-2 | Sandsnston | qtz-chl-ill-cal | 10 cm | qtz | – | | | + 14.8 | – 7.9 | |
| T-1 | Siltstone | qtz-chl-ill-chl/sm-cal-dol-py | 80 cm | | | | | + 17.5 | | |

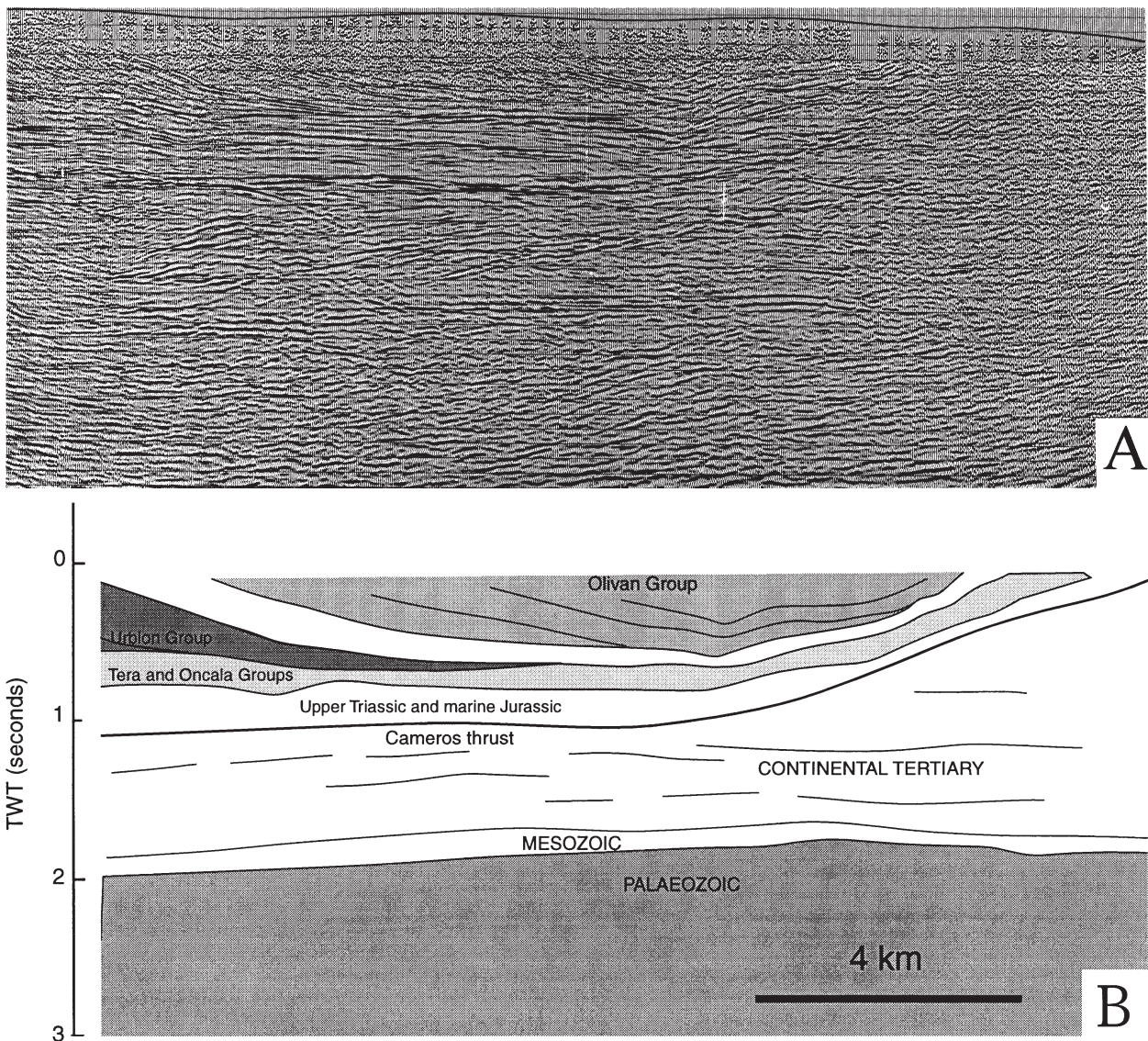


Fig. 4. Seismic reflection profile and interpretation of the central part of the Cameros Massif. Cross-section Fig. 1.

of bed-parallel cleavage in lutites associated with pinch-and-swell structures follows the shape of the sandstone beds (Fig. 5B). This kind of structure is found in areas which were presumably deeply buried within the basin-fill (Fig. 2). The calculated amounts of extension cannot be extrapolated to the whole of the basin, but they give an idea about the difference in extensional deformation between the different stratigraphic levels, and the mechanisms of deformation involved during the extensional processes in the synrift sequence. The increase in vein density and extension from the upper to the lower part of the sedimentary series, and the perpendicularity between beds and veins, suggest a mechanism of bending, with extension at the external hinges, for the formation of the main extensional syncline (Figs 2 and 3). This mechanism agrees with the wedge geometry of the synrift sequence (Fig. 3), with differences in dip of more than 30° from the upper to the lower part of the sedimentary series (Casas-Sainz & Gil-Imaz, 1998).

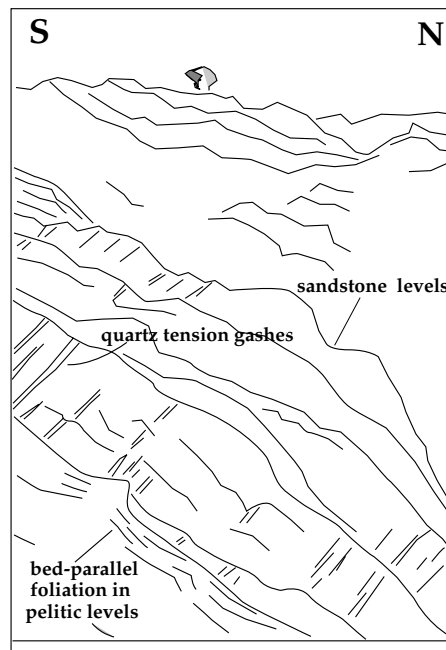
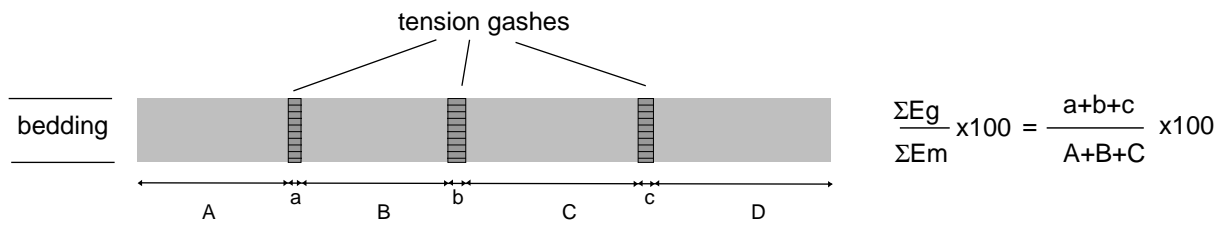
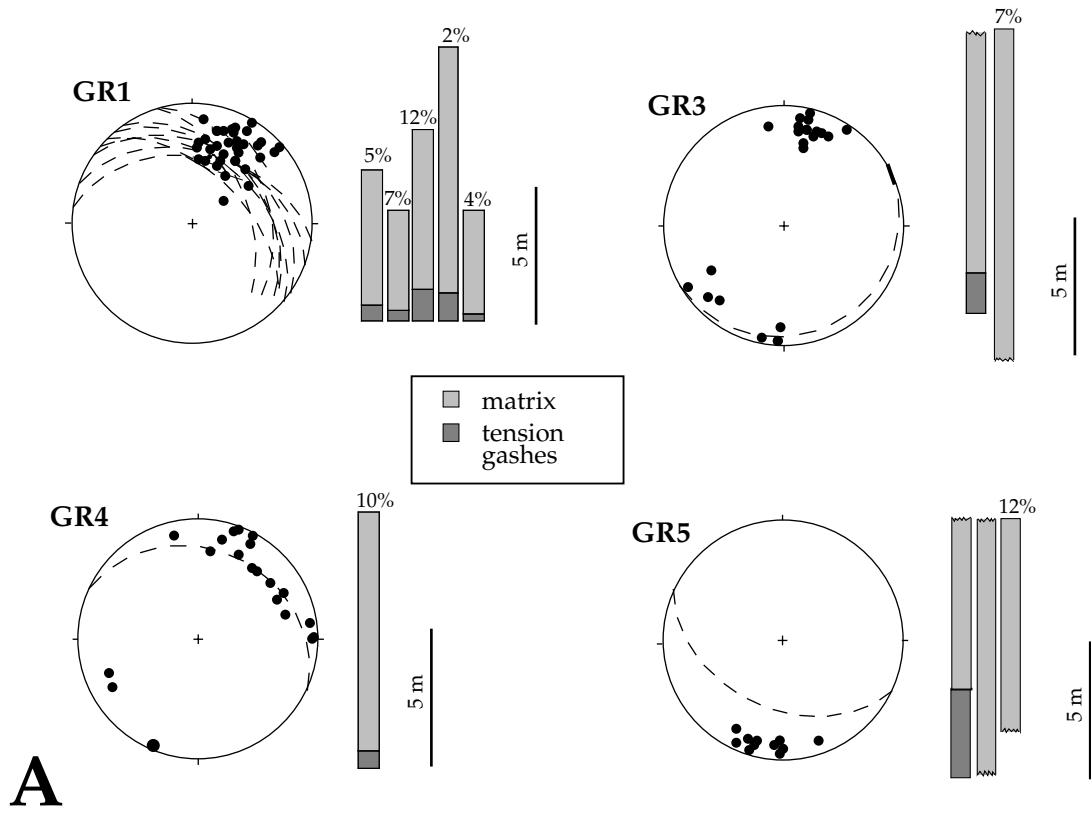
PALAEOTHERMAL ANALYSIS

Vein composition

Optical, XRD and microprobe analysis reveal that veins are almost invariably quartz with minor calcite and albite. Table 1 shows the mineralogy of the veins and host rocks. Quartz is present as milky and prismatic and fibrous crystals filling veins in quartz-rich sandstones. The size of quartz crystals ranges from millimetres to 25 cm at site GR5 (Pégado anticline). Chlorite, muscovite and albite are also locally present near the contact of the host rock or in the vein. EMPA of chlorite and muscovite in veins is shown in Table 2. Pyrite and titanium oxide crystals have been found as sporadic minor constituents.

Fluid inclusion study

Data were acquired from 10 different veins; nine of them located at the central sector of the basin and one from the



south-eastern part (GR5 site, Fig. 2). All the inclusions studied are hosted in quartz crystals. Their classification is based on the number of phases observed at room temperature and on estimates of the fluid composition determined by observation of phase changes during preliminary heating and freezing runs. Three types of inclusions have been found:

(a) Type I: NaCl–H₂O biphasic at room temperature (liquid and vapour), with vapour to liquid ratios between 0.1 and 0.2 and sizes from 5 to 70 μm , with regular shape.

(b) Type II: NaCl–CO₂(+N₂)–H₂O triphasic and biphasic at room temperature (two liquids and vapour or liquid and vapour), with vapour to liquid ratios between 0.2 and 0.3 and sizes from 3 to 50 μm . They are more regular in shape than Type I and mainly negative crystals.

(c) Type III: biphasic with a liquid (its refraction index gives a dark colour) and a gas bubble, with morphology and size similar to those of Type II inclusions.

Microthermometric data were obtained from Type I and II inclusions based on the occurrence in single crystals showing evidence of growth zonation. The inclusions appear as subparallel groups, particularly with different concentrations in adjacent zones. Using microthermometric techniques together with Raman spectrometry analyses, it is possible to find the composition and total homogenization temperatures for Type II inclusions. Raman analyses of 21 inclusions from samples U-1, U-2 and U-4 indicate that the carbonic phases of these fluid inclusions are mixtures dominated by CO₂ with some amounts of N₂. The CO₂/N₂ ratio changes from 1:0 to 1:0.25. For Type I inclusions, measured eutectic temperatures between –29 °C and –23 °C indicate a system with H₂O and NaCl as components. Figure 6 displays the histograms of T_{mi} vs. T_{h} and T_{mi} vs. T_{h} diagrams.

Microthermometric data (Table 1) show a net decrease in homogenization temperature up sequence, from a mean temperature of 223 °C in sample T-3 to 107 °C in sample O-1. Comparing samples from the same sector, a similar behaviour is found: U-1 is the lowermost sample in the central area with a mean T_{h} of 208 °C, one hundred degrees higher than the uppermost sample of the same sector, O-1. Without considering changes in real entrapment temperature due to changes in pressure, there is a linear correlation between the T_{h} obtained and the position of samples within the stratigraphic log. The correlation curve (Fig. 7) indicates a gradient of 27 °C km⁻¹, assuming that this correlation is linear, as it occurs in the upper levels of the crust, not considering variations due to the different thermal conductivity of rocks. If this linear correlation is assumed, there must be an eroded section of at least 1500 m, in order to obtain a surface temperature within an acceptable range.

The real temperature of fluid inclusion formation can be calculated approximately if a pressure can be obtained from an independent source. In our case, this pressure can be estimated according to the burial depth of each sample, assuming (i) that the position within the stratigraphic column coincides with this depth and (ii) that the minimum eroded section can be calculated according to the linear temperature gradient as explained in the previous paragraph. Pressure corrections of homogenization temperatures were calculated for molar volumes of 21 mL mol⁻¹ and 20 mL mol⁻¹, for a composition $X_{\text{H}_2\text{O}}=0.941$, $X_{\text{CO}_2}=0.040$, $X_{\text{NaCl}}=0.0185$. This composition is the most similar to the analysed inclusions

Table 2. Electron microprobe analysis of chlorite, chloritoid, muscovite and albite. Cations for chlorite and mica calculated on the basis of O₁₀(OH)₈, and O₁₀(OH)₂, respectively. All iron as Fe²⁺.

| | Host rock | | Vein | | |
|--------------------------------|-----------|--------|-------|-------|--------|
| | Chl | Ctd | Chl | Mc | Alb |
| SiO ₂ | 21.84 | 24.48 | 22.84 | 46.84 | 69.37 |
| Al ₂ O ₃ | 23.76 | 39.96 | 25.23 | 36.18 | 20.03 |
| FeO | 37 | 26.82 | 33.5 | 1.33 | 0 |
| MgO | 4.86 | 0.57 | 6.74 | 0.21 | 0 |
| MnO | 0.14 | 0.46 | 0.16 | 0 | 0 |
| NiO | 0.08 | 0 | 0 | 0 | 0 |
| Cr ₂ O ₃ | 0 | 0.05 | 0.01 | 0 | 0 |
| TiO ₂ | 0.05 | 0.02 | 0.04 | 0.02 | 0.04 |
| Na ₂ O | 0.01 | 0 | 0 | 0.81 | 12.26 |
| K ₂ O | 0.02 | 0.03 | 0.01 | 8.74 | 0.02 |
| CaO | 0 | 0 | 0.01 | 0.03 | 0 |
| H ₂ O | | | 11.01 | 4.52 | |
| tot | 87.76 | 92.387 | 99.72 | 98.87 | 101.75 |
| Si | 2.46 | 1.02 | 2.49 | 3.11 | 2.98 |
| Al(IV) | 1.54 | | 1.51 | 0.89 | 0 |
| Al(VI) | 1.62 | | 1.73 | 1.94 | 0 |
| Al(T) | 3.16 | 1.97 | 3.24 | 2.83 | 1.02 |
| Fe | 3.49 | 0.94 | 3.05 | 0.07 | 0 |
| Mg | 0.82 | 0.04 | 1.09 | 0.02 | 0 |
| Mn | 0.01 | 0.94 | 0.02 | 0 | 0 |
| Ni | 0 | 0 | 0 | 0 | 0 |
| Cr | 0 | 0 | 0 | 0 | 0 |
| Ti | 0 | 0 | 0 | 0 | 0 |
| Na | 0 | 0 | 0 | 0.1 | 1.02 |
| K | 0 | 0.02 | 0 | 0.74 | 0 |
| Ca | 0 | 0 | 0 | 0 | 0 |
| Fe/(Fe+Mg) | 0.81 | 0.96 | 0.74 | – | – |

Fig. 5. A. Orientation (Schmidt projection, lower hemisphere) of tension gashes in the eastern Cameros Massif at some of the sites in which samples for palaeothermometric studies were taken (location in Fig. 1). The stereoplots show the poles of tension gashes (black circles) and bedding surfaces (great circles in broken lines). The histograms show the amount of extension due to vein formation at the different outcrops studied, and different strata within the same outcrop. The sketch below indicates the way extension is calculated. B. Field aspect (photograph and sketch) of quartz tension gashes and pinch-and-swell structures at the base of the Urbión Group (site GR1 in Fig. 2A).

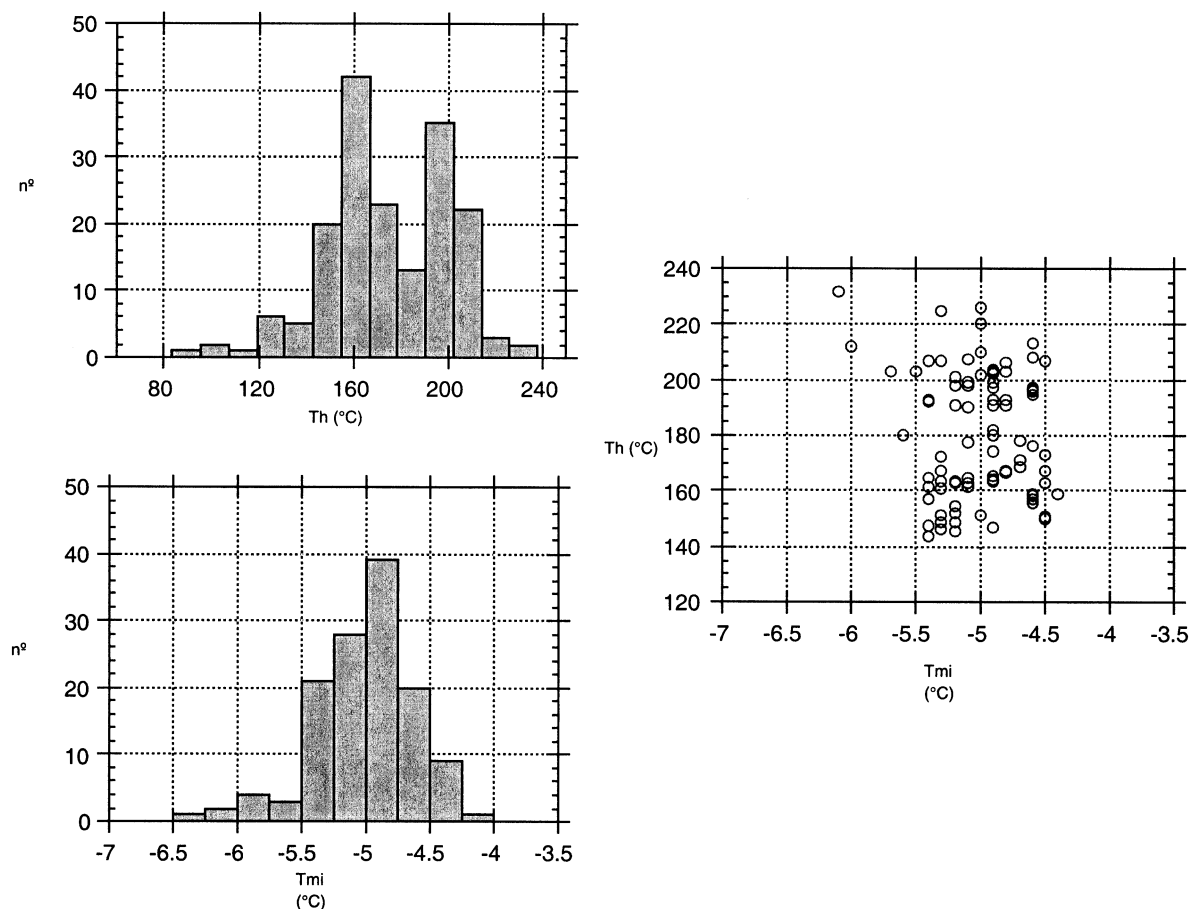


Fig. 6. A. Histograms of melting ice temperature (T_{mi}) and homogenization temperature (T_h) of the studied samples. B. T_{mi} plotted against T_h .

for which experimental data exist (Gehrig, 1980). Isochores of inclusions with NaCl were obtained according to the state equations given by Bodnar & Vityk (1995) included in program MacFinclor by Brown & Haggeman (1995). The results obtained (Fig. 7) agree with a linear temperature gradient of $41\text{ }^{\circ}\text{C km}^{-1}$, and are consistent with the eroded section inferred from the noncorrected temperatures. Although these temperatures must be taken cautiously, they allow us to constrain the gradient during fluid inclusion formation between 27 and $41\text{ }^{\circ}\text{C km}^{-1}$.

There is a perceptible spatial distribution of inclusion type in the stratigraphic sequence. Samples located at the bottom of the Urbión Group always contain Type II inclusions. In samples U-4 and U-3, Type I and II (biphasic) inclusions coexist in a single crystal. Although both types of inclusions are located at the bottom of the crystal, and are considered as primary, they are not found in the same bands. The difference in the fluid composition can be interpreted as a consequence of changes in host mineralogy of the veins. Close samples, below within the stratigraphic series, have only Type II and above have only Type I.

In samples U-4 and U-3 the homogenization temperature of the Type I (170 and 180 °C) is always lower than

Type II (200 and 245 °C); if both types are considered primary inclusions, these T_h differences can be used to calculate the minimum pressure of formation for them. Using Bodnar & Vityk's (1995) equation for the NaCl–H₂O system and Bowers & Helgeson's (1983) for the NaCl–H₂O–CO₂ system, the difference in temperature found between the two types of inclusions corresponds to a minimum pressure of about 0.6 and 1.1 kbar, respectively.

From melting ice temperature (Table 1 and Fig. 6) no important changes in salinity are obtained. Values range from 7.7 to 10 Wt% NaCl for samples containing Type I inclusions. T-3 sample hosted in siltstone has the highest and U-9 hosted in limestone the lowest. This apparent homogeneity seems to be in conflict with a local fluid source although these salinities are in accordance with those observed in other detrital basins (Hanor, 1979). Nevertheless, samples with sandstone as host rocks, have the same salinity.

Isotopic data

Values of isotopic composition of water and minerals show a wide dispersion (see Table 1 and Fig. 8). The

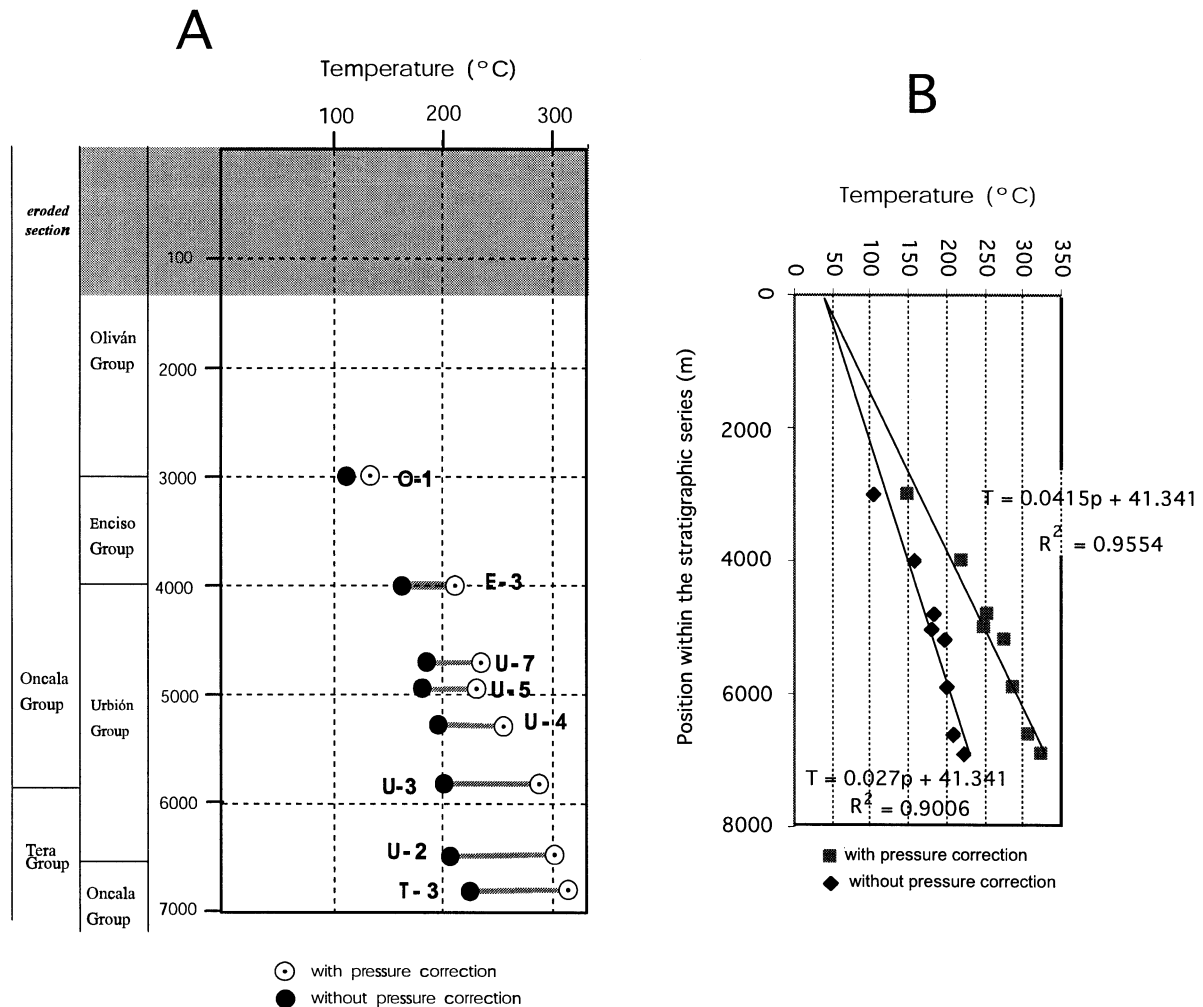


Fig. 7. A. Temperatures obtained from fluid inclusions in the samples studied, plotted against their depth, according to the stratigraphic column, with and without pressure correction (see text for explanation). B. Linear regression curves for the noncorrected and corrected temperatures.

$\delta^{18}\text{O}$ of quartz ranges from +26 to +16.60‰. According to the T_h values measured, and based on the quartz–water fractionation equation of Clayton *et al.* (1972), the calculated $\delta^{18}\text{O}$ of water in equilibrium with quartz ranges from +1 to +10.0‰. Samples U-1 to U-10 were obtained from the same central sector of the Cameros Basin. Samples U-1 to U-7 show a direct correlation between the $\delta^{18}\text{O}$ value of water in quartz with depth of burial (assuming that it is equivalent to the position in the stratigraphic sequence, see Fig. 7). This is in agreement with a local isotopic buffering of fluids, since homogeneous values should be expected if large-scale fluid flow was involved. However, it should be noted that samples U-10 and U-9 do not plot on this trend.

The highest $\delta^{18}\text{O}$ values of water are found in samples hosted in limestone and calcareous siltstone (T3 and E1), which is inconsistent with an influence of $\delta^{18}\text{O}$ -rich phases as carbonate minerals on isotopic water composition.

Calcites show quite constant $\delta^{13}\text{C}$ values of about -8‰ , except for sample U-8 which has a value slightly

higher (-5‰), but variable $\delta^{18}\text{O}$ values between +14.8 and +22.1‰. Both the lowest and the highest $\delta^{18}\text{O}$ value of the mineral are found in veins hosted in sandstone. Low $\delta^{13}\text{C}$ values indicate an influence of organic carbon in the fluid. The highest $\delta^{13}\text{C}$ value is found in a sample hosted in siltstone.

Lack of suitable fluid inclusions for microthermometric studies precludes evaluation of the water isotopic composition. Quartz coexisting with calcite shows an almost constant value of $\delta^{18}\text{O}$ whereas $\delta^{18}\text{O}$ in calcite varies from +22.1 to +15.3‰. Using Sharp & Kirchner's (1994) empirical calibration equation, $171 \pm 15^\circ\text{C}$ is obtained for the pair of U-10, and negative temperatures for the two other pairs (U-6 and U-9). Although no suitable fluid inclusions for microthermometric studies were found in these samples, the negative values for temperature from isotopic geothermometers clearly point to a nonequilibrium between quartz and calcite. Finally, the high $\delta^{18}\text{O}$ values for these calcites seem to indicate a major contribution of $\delta^{18}\text{O}$ -rich phases to a late and low-temperature fluid.

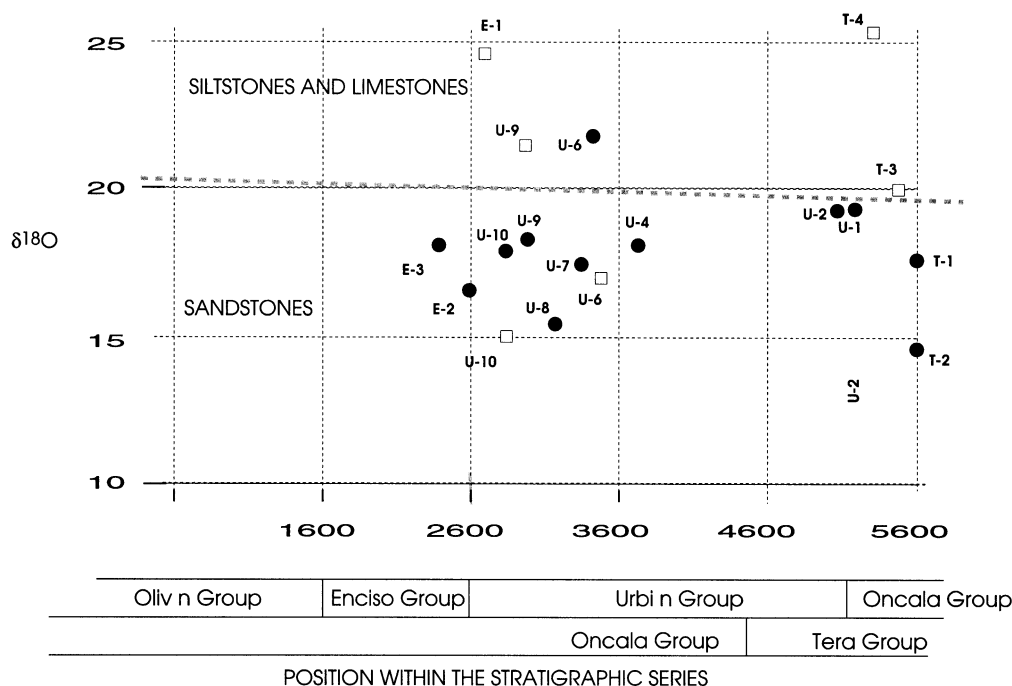


Fig. 8. Oxygen isotopic values of silica (circles) and calcite (open squares) as a function of depth and position within the stratigraphic series.

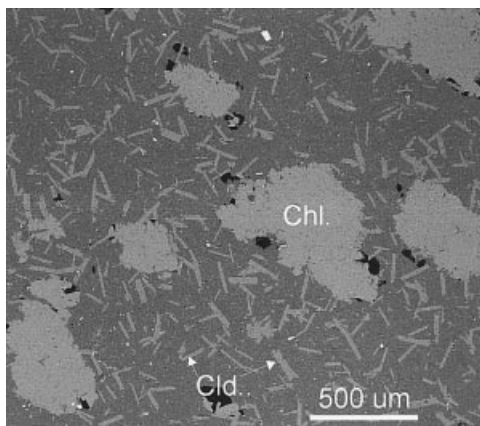


Fig. 9. Backscattered scanning electron photograph of the mineral assemblage (i), where chloritoid and chlorite crystals can be seen.

Mineral assemblages

On the basis of mineral assemblages (Table 1 and Fig. 9), a prograde sequence from deep diagenesis to epizone can be defined for the rocks of the Cameros Basin. This tendency has been previously described on the basis of illite crystallinity and mineralogical studies (Guiraud & Séguret, 1984; Goldberg *et al.*, 1988; Alonso-Azcárate *et al.*, 1995; Barrenechea *et al.*, 1995; Mata, 1997).

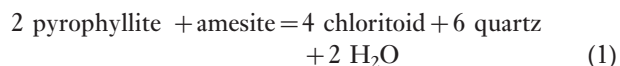
The mineral assemblages from the bottom to the top of the sequence in the CV section are:

- (i) quartz + chlorite + muscovite + paragonite + chloritoid ± calcite ± albite

- (ii) quartz + chlorite + muscovite ± paragonite ± pyrophyllite ± calcite ± albite ± chlorite/smectite
- (iii) quartz + chlorite + muscovite ± smectite ± illite/smectite ± albite

The highest-grade mineral assemblage (i) is present in GR1 site (deepest strata within the Mesozoic Basin exposed at surface) and can also be found in a NW–SE-orientated area from GR1 to GR5 sites (Fig. 2). Paragonite and chloritoid disappear up sequence and sporadic pyrophyllite is detected. Large poikiloblastic pyrite crystals (up to 20 cm in length) have also been described in assemblages (i) and (ii) together with the assemblage: cookeite (Al–Li-rich chlorite) + rectorite + kaolinite + barite, probably related with the pyrite deposit (Mata *et al.*, 1998; Alonso-Azcárate *et al.*, 1999) due to syn- to post-hydrothermal overprinting. Assemblage (iii) is found in the upper strata of the Enciso and Oliván Groups. Although illite crystallinity data (Alonso-Azcárate *et al.*, 1995; Barrenechea *et al.*, 1995) show values typically in the range from epizone to diagenetic conditions, interference of the (001) reflection of paragonite can distort the true IC value in paragonite-bearing rocks (Frey, 1987, and references therein).

Therefore, metamorphic conditions are based on the reaction



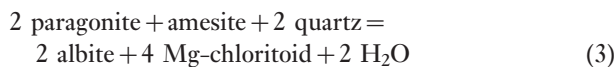
which can be calculated from coexisting phases of the above mentioned assemblages.

Representative chemical composition on the basis of EMPA of coexisting chloritoid, chlorite and pyrophyllite are shown in Table 2. Figure 9 shows a BSE image where

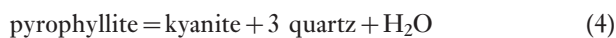
random chloritoid crystals and chlorite crystals can be seen. The P - T conditions for assemblage (i) among the amesite, Mg-chloritoid, quartz and H_2O phases have been calculated with the program THERMOCALC v2.5 and the database of Holland *et al.* (1998). The activities of these phases were calculated on an ideal basis by using the program AX (Holland 1992, written communication). These calculations yield a minimum temperature of 300–350 °C over a pressure range of 1–6 kbar for assemblage (1). The reaction:



was used to constrain an upper pressure limit through the absence of jadeite at ≈ 6 –7 kbar at 300–350 °C. An upper temperature limit was calculated by using the reaction



due to the absence of albite in some samples and by the reaction



since kyanite is not stable.

The previous calculations indicate that temperature ranges between 300 and 350 °C in a pressure range of 1–6 kbar. These data suggest that at least 350 °C was reached for strata buried at 5600 m minimum depth.

DISCUSSION

Factors controlling vein formation and composition source of fluids

Field and structural data along a continuous stratigraphic sequence from the Oliván Group to the Urbión Group show that veins are concentrated in the deepest areas of the basin or the lower sections within the stratigraphic units, being almost absent in upper stratigraphic units. The presence of veins shows that extensional deformation took place and boudinage can be observed. Geometrical relations between strata and veins (almost perpendicular, and veins with a constant direction) suggest an extensional origin. The strike of veins coincides with the strike of the main normal faults limiting the basin to the north and south (Guimerà *et al.*, 1995; Casas-Sainz & Gil-Imaz, 1998) and also with the strike of metric to hectometric faults contemporary with the Early Cretaceous extension (Guiraud, 1983; Casas-Sainz & Gil-Imaz, 1998). All these data are consistent with a NNE–SSW extension direction and point to an extensional origin for the vein-fills analysed in this study.

The base of the Urbión group, where the larger veins are located (Fig. 5b), is composed of ≈ 50 m of fluvial, channellized quartz-rich sandstones overlying a limestone sequence and it is overlain by a > 3000 -m-thick sequence of pelitic–psammitic strata. Brittle behaviour, chemical composition of sandstones and abrupt

permeability changes between the overlying lutitic strata and the sandstones seem to have conditioned the formation of the broader, deeper veins and the fluid migration within the veins.

On the other hand, and on the basis of fluid inclusion and isotopic data, a local origin for the fluids can be suggested. Inclusions types correlate mainly with the lithology of the different units. Moreover, the results of fluid inclusion analyses indicate a correlation between the stratigraphic level in which the samples were taken and the homogenization temperature, even when no pressure correction is applied (Fig. 7). Varied calculated isotopic water compositions support the idea of a local fluid flow resulting in isotopic buffering of fluids at the basin scale, since a homogeneous value should be found with large-scale fluid flow. The highest $\delta^{18}O$ value of water coincides with the samples hosted in limestone and siltstone in accordance with an influence of $\delta^{18}O$ -rich phases as carbonate minerals on isotopic water composition. Fluid inclusion entrapment should represent the temperature of the extensional interval since inclusions can be considered as primary in origin.

As a conclusion, the geometry of veins is related to the stages of filling of the basin with moderate to high loads. Fluid flow may have occurred on a local scale of tens of metres, confined to individual packets of sandstone and shale in the deepest areas of the basin. This mechanism has been proposed in similar geological environments by Cartwright *et al.* (1994) to explain the formation and origin of fluid in veins and their relations with the tectonic evolution, explaining vein formation as the result of local processes.

The magnitude of the fluid flow during the diagenetic evolution of this sedimentary basin is also a useful indicator of the origin of the low-grade mineral assemblages. Casquet *et al.* (1992) and Barrenechea *et al.* (1995) suggested a fluid-controlled metamorphism, or hydrothermal metamorphism, in a quartz-rich area where many of the veins are found. In contrast, we suggest that for the first diagenetic stages of the evolution of the Cameros Basin, thermal equilibrium between fluid and rock is likely, owing to the existence of localized flow. However, caution is needed when temperatures from extensional gashes are used to calculate temperatures for a later metamorphic event. The mineral assemblages indicate higher temperatures than those obtained from fluid inclusion studies and these higher temperatures are related to a later thermal event. Moreover, in the Cameros Basin, the mechanism of local-scale fluid mobilization seems to have occurred in different episodes to explain the pyrite deposits that occur in other areas of the basin where sulphide deposits are restricted to a single high-permeability sandstone aquifer (Alonso *et al.*, 1999).

Cretaceous geothermal gradient evolution

An initial approach to calculate the palaeothermal gradient was made by plotting the temperature obtained

from fluid inclusions against the depth of the samples, obtained from their position in the stratigraphic log of the basin fill (Fig. 7). This is the model used normally when thermal gradients are obtained from borehole data (Hagen & Surdam, 1989; Jensen & Doré, 1993; Lerche, 1993; Green *et al.*, 1995) and allows for the variations of gradient in a vertical section to be determined. Variations with respect to a linear pattern are caused by the differences in thermal conductivity of the different stratigraphic units (Blackwell & Steele, 1989). Determination of the geothermal gradients also allows the eroded sections of the basin to be estimated, considering that the slope of the depth–temperature plot can be extrapolated from the truncation point to the surface (Magara, 1976; Green *et al.*, 1995). In the example studied, the Tertiary inversion of the basin, forming a large syncline over the thrust surface, allows an inclined section of the basin to be exposed at the surface (Fig. 3). If we assign depths to the sample sites as a function of their stratigraphic position within the sedimentary sequence, a temperature–depth diagram can be drawn (Fig. 7). The slope of the regression line is the palaeothermal gradient obtained from the fluid inclusions analysed in this work. As we pointed out, this gradient must be between 27 °C km^{-1} and 41 °C km^{-1} (Fig. 7), and allows us to infer an eroded section of at least 1500 m.

The mineral assemblage at the top of the Oliván Group, sample O-1 (Table 1) suggests that the evolution of these rocks corresponds to deep diagenesis and they were buried possibly by more than 1 km, which is consistent with the results obtained. The palaeotemperatures obtained can be explained by a normal or slightly elevated geothermal gradient. These quasi-normal gradients are consistent with models involving low sedimentation rate (McDonald *et al.*, 1989; Ter Voorde & Bertotti, 1994), such as the one inferred in the Cameros Basin during the Early Cretaceous (about 0.25 mm yr^{-1} on average).

From P – T calculations on the basis of mineral assemblages, temperatures between 300 and 350 °C and pressures of less than 2 kbar were reached at depths between 5000 and 6000 m within the basin sedimentary fill. K-white mica dimensions (Mata, 1997) range from 8.98 to 9.00 Å in shales and sandstones of the Urbión, Enciso and Oliván groups and are indicative of a low-pressure geotectonic setting. Both mineralogical and textural characteristics of these rocks are typical of extensional low-grade settings where shale- and sandstone-rich sequences are buried and folded in passive margins (Merriman & Frey, 1999). Assuming that the increase in temperature was related to an increase in the geothermal gradient, a palaeothermal gradient of $\approx 70\text{ °C km}^{-1}$ can be inferred. Both gradient and temperatures obtained from mineral parageneses are higher than those obtained from fluid inclusions for the same point, which implies a heating event between the end of the basin filling (probably early Albian, Muñoz *et al.*, 1997) and the age of the metamorphic peak

(100 Ma, late Albian to Cenomanian), with the formation of the highest grade assemblages. Between the two stages, a cleavage-forming folding stage took place (Casas-Sainz & Gil-Imaz, 1998). Observations in thin sections show that chloritoid crystals are randomly orientated in a strongly orientated matrix and cut across the cleavage planes (Casas-Sainz & Gil-Imaz, 1998). This textural relationship indicates, at the regional scale, that the metamorphic peak post-dates both the extensional, subsiding stage and also the cleavage-related folding. Evidence of a heating event at the end of the Early Cretaceous is also found in the central part of the Iberian Chain, where it can be related to a generalized remagnetization event (Juárez *et al.*, 1994, 1998). The North Pyrenean zone, located 100 km NE of the studied area (Fig. 1), also records a heating event (thermal metamorphism) dated at $\approx 90\text{ Ma}$ (Albarède & Michard-Vitrac, 1978). This implies that thermal metamorphism responsible for the low-grade mineral assemblage in the Cameros Basin had a regional significance in the NE part of the Iberian plate. Nevertheless, more data are still needed, especially in the Iberian Chain, to clearly correlate these events with the low-grade metamorphism in the Cameros Basin.

The increase in temperature and geothermal gradient during the Early Cretaceous, recorded by the increasing temperature of mineral parageneses (350 °C) with respect to fluid inclusions, is consistent with models of lithospheric stretching and crustal thinning during rifting (Royden *et al.*, 1980). Re-equilibration of isotherms after the rifting stage (Late Cretaceous) and crustal thickening (Late Eocene to Oligocene, Casas *et al.*, 2000) probably caused the cooling of the upper crust and the normal gradient to be recovered. The final stages in the thermal evolution correspond to the Tertiary exhumation of the whole basin (Fig. 2).

Implications for the geometry of the sedimentary basin

The two models of the Mesozoic geometry of the Cameros Basin can be summarized as follows (Fig. 10):
 1 The lateral superposition model envisages a sag-basin formed above a ramp of a nonoutcropping normal fault, located at several kilometres depth within the continental crust (Fig. 10). The top-to-the-south movement of the hangingwall created accommodation, progressively filled by synextensional basinal deposits. The maximum thickness of sediments is limited by the vertical distance between the two flats of the normal fault. The final geometry of the synrift deposits would be an extensional sedimentary wedge resulting from the northward migration of the depocentre during the rifting stage (Guiraud & Séguret, 1984; Mas *et al.*, 1994; Guimera *et al.*, 1995) with onlap to the north of the sedimentary sequences on the prerift strata (Fig. 10). In this model the northward dip of the synrift sequence at the southern limb of the

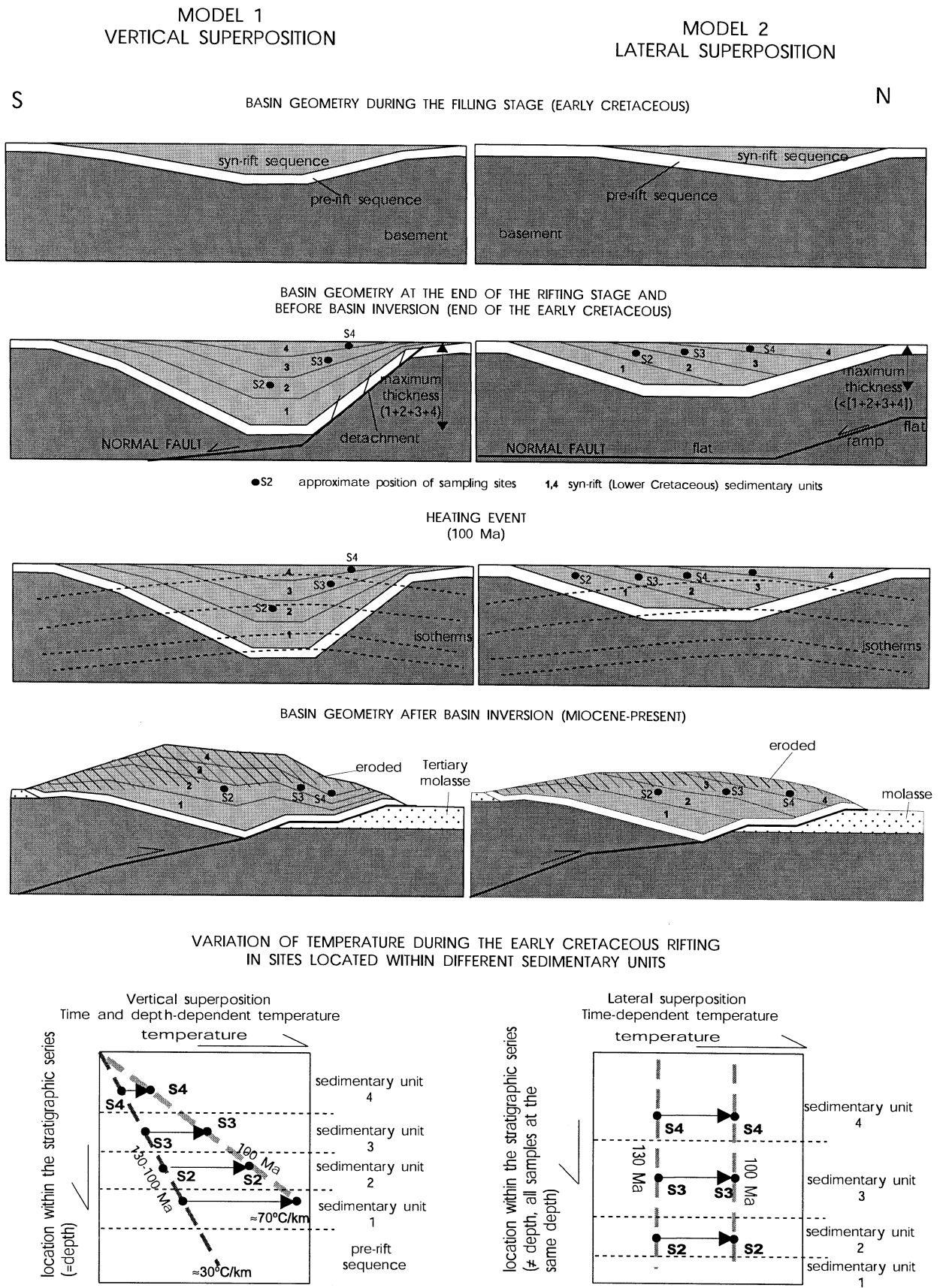


Fig. 10. Comparison between the geometry of the two basin models (lateral and vertical superposition of sedimentary bodies) proposed for the Cameros Basin. The approximate location of samples within the basin is shown for the two models. In the lower part the palaeotemperatures at the different stratigraphical units are shown (schematic).

Northern Cameros syncline (Fig. 2) was acquired during or immediately after the deposition of each sedimentary unit. The final true thickness of the Mesozoic basin did not exceed 5 km, and the depth at which the rocks exposed at the surface were buried was less than 2 km (Fig. 10). According to this model, the palaeotemperature recorded in each unit would not be dependent on their stratigraphical position but only on the temperature increase with time; for a given geothermal gradient all the samples along the sampling section would have been subjected to the same P - T conditions at a given time.

2 The vertical superposition model is based on a normal fault in the Palaeozoic basement, cross-cutting the whole upper crust with a listric geometry at depth (Casas *et al.*, 2000). The prerift sedimentary cover is detached from the basement by the Upper Triassic evaporites, and is stretched by smaller scale normal faults. In an overall view the filling of the basin forms a large asymmetrical syn-sedimentary syncline (Casas-Sainz & Gil-Imaz, 1998), its axis lying south of the present-day position of the Northern Cameros syncline (Fig. 10). This implies that during the extensional stage, the prerift and the synrift strata were passively folded by bending above the listric normal fault toward the central part of the basin (hypothesis considered in the cross-section of Fig. 3). This process would result in maximum extension of beds in the hinge zone of the syncline, which crop out along a band from GR1 site to the GR5 site. This outcrop, where the highest density of tension gashes and pinch-and-swell structures occur, coincides with the occurrence of the chloritoid paragenesis. The maximum thickness of synrift sediments at the basin centre (about 1 km of Mesozoic prerift deposits and 8 km of synrift deposits) is consistent with the occurrence of metamorphic assemblages indicating pressure conditions between 1 and 2.3 kbar (4–9 km) in the centre of the basin. Toward the north-west and south-east the thickness of these units decreases gradually (Casas-Sainz, 1993). The timing of extensional bending, and also of vein formation, would be late with respect to the main normal faults at the northern basin margin (Fig. 3), considering that fluid inclusions have a primary origin.

The thermal evolution of the Cameros Basin, determined from fluid inclusions and mineral parageneses, constrains the reconstruction of the initial geometry of the basin. The main consequence is that temperature increases with depth and with the stratigraphic position within the basin. Therefore, the results obtained from the study of fluid inclusions and mineral assemblages argue in favour of the second of the models proposed (Fig. 10), since there are differences in palaeotemperatures from the upper to the lower part of the sedimentary sequence. The location of highest-grade mineralogical assemblage is also consistent with this hypothesis. Casquet *et al.* (1992) argued for circulation of fluids as proposed by Oliver (1986) along a NW–SE shear zone to account for the anomalous geothermal gradient in the central part of the basin. This hypothesis implies a horizontal thermal

gradient, with temperatures increasing southward. Nevertheless, and according to the reconstruction of the basin geometry in the two models presented (Fig. 3), the large faults channelling fluid circulation (and therefore the heat source) are located north of the area studied. This is contrary to the evidence of increasing pressure/temperature conditions from north to south through the southern limb of the Cameros syncline.

CONCLUSIONS

The extensional Cameros Basin, formed between the Late Jurassic and the Albian along the northern margin of the Iberian plate, shows an asymmetric shape with fault-controlled margins between E–W and NW–SE directions. During extension, tension gashes with quartz and calcite composition formed in the synrift sequence, parallel to the master faults limiting the basin, the amount of extension accomplished by the veins being higher the lower in the stratigraphic section. A thermal event, giving rise to an anomalous geothermal gradient, is necessary to explain the low-grade mineralogical assemblage of chloritoid, chlorite and paragonite in the deepest area within the basin outcropping at present. Thus, an increasing gradient from the extensional stage (between the Late Jurassic and the Albian), to the thermal peak (100 Ma) can be identified. Palaeotemperatures from fluid inclusions are representative of the extensional stage and mineralogical assemblages in the host rock are the result of the thermal equilibration at the thermal peak. Fluid composition and isotopic analysis of quartz and calcite in veins point to a local origin of fluids within the basin and need not reflect large-scale fluid circulation. The present-day geothermal gradient has probably prevailed since the end of the Cretaceous thermal event. The Cretaceous heating event can be correlated with a more general event that took place in the north-eastern part of the Iberian plate.

Comparative studies of palaeothermal, mineralogical and structural data allow us to constrain basin models. The results obtained for the reconstruction of the Mesozoic basin suggest the vertical superposition of the synrift sedimentary sequences, over a steep basin-bounding normal fault, with a maximum thickness of the synrift deposits of about 8 km.

ACKNOWLEDGMENTS

This work was supported by project PB97-0997 of the Dirección General de Enseñanza Superior (Spain). We thank Peter Tropper and Carl Henderson of the Department of Geological Sciences of the University of Michigan for helping with the thermodynamic calculations and Scanning Electron Microscope. M. del Mar Abad Ortega (Servicios Centrales of the University of Granada, Spain) helped with the Electron Microprobe

Analysis. We also thank to Z. Sharp and E. Cardellach for their help in the isotope analysis and R. Merriman and an anonymous referee for the reviews of this manuscript.

REFERENCES

- ALBARÈDE, F. & MICHARD-VITRAC, A. (1978) Datation de métamorphisme des terrains secondaires des Pyrénées par les méthodes ^{39}Ar - ^{40}Ar et ^{37}Rb - ^{87}Sr ; ses relations avec les péridotites associées. *Bull. Soc. Géol. Fr.*, **20**, 681–687.
- ALLEN, P.A. & ALLEN, J.R. (1990) *Basin Analysis: Principles and Applications*. Blackwell Science, Oxford.
- ALONSO-AZCÁRATE, J., BARRENECHEA, J.F., RODAS, M. & MAS, R. (1995) Comparative study of the transition between very low-grade and low-grade metamorphism in siliciclastic and carbonate sediments: Early Cretaceous, Cameros Basin (Northern Spain). *Clay Minerals*, **30**, 407–419.
- ALONSO-AZCÁRATE, J., RODAS, M., BOTTRELL, H., RAISWELL, R., VELASCO, F. & MAS, J.R. (1999) Pathways and distances of fluid flow during low-grade metamorphism: evidence from pyrite deposits of the Cameros Basin, Spain. *J. Metamorphic Geol.*, **17**, 339–348.
- ALVARO, M., CAPOTE, R. & VEGAS, R. (1979) Un modelo de evolución geotectónica para la Cadena Celtibérica. *Acta Geol. Hisp.*, **14**, 172–177.
- ANDREWS-SPEED, C.P., OXBURGH, E.R. & COOPER, B.A. (1984) Temperatures and depth-dependent heat flow in Western North Sea. *A.A.P.G. Bull.*, **68**, 1764–1781.
- ANGELIER, J. (1994) Fault slip analysis and palaeostress reconstruction. In: *Continental Deformation* (ed. by P.L. Hancock), pp. 53–100. Pergamon Press, Oxford.
- Aoyagi, K. & ASAKAWA, T. (1984) Paleotemperature analysis by authigenic minerals and its application to petroleum exploration. *A.A.P.G. Bull.*, **68**, 903–913.
- ARCHE, A. & LÓPEZ-GÓMEZ, J.V. (1996) Origin of the Permian-Triassic Iberian Basin, central-eastern Spain. *Tectonophysics*, **266**, 443–464.
- ARTHAUD, F., MÉGARD, F. & SÉGURET, M. (1977) Cadre tectonique de quelques bassins sédimentaires. *Bull. Centres Rech. Explor. Prod. Elf-Aquitaine*, **1**, 147–188.
- ARTHAUD, F. & SÉGURET, M. (1972) Sur l'origine tectonique de certains joints stylolitiques parallèles à la stratification: leur relation avec une phase de distension (exemple du Languedoc). *Bull. Soc. Géol. Fr.*, **7**, 12–17.
- AURELL, M., MELÉNDEZ, A., SANROMÁN, J., GUIMERÀ, J., ROCA, E., SALAS, R., ALONSO, A. & MAS, R. (1992) Tectónica sinsedimentaria distensiva en el límite Triásico-Jurásico en la Cordillera Ibérica. *Procc. III Congreso Geológico España Y VIII Latinoamericano Geología*, **1**, 50–54.
- BARRENECHEA, J.F.F., RODAS, M. & MAS, J.R. (1995) Clay minerals variations associated with diagenesis and low-grade metamorphism of Early Cretaceous sediments in the Cameros Basin, Spain. *Clay Minerals*, **30**, 119–133.
- BLACKWELL, D.D. & STEELE, J.L. (1989) Thermal conductivity of sedimentary rocks: measurement and significance. In: *Thermal History of Sedimentary Basins: Methods and Case Histories* (ed. by N.D. Naeser & T.H. McCulloh), pp. 13–36. Springer-Verlag, New York.
- BODNAR, R.J. & VITYK, M.O. (1995) Interpretation of microthermometric data for H_2O - NaCl fluid inclusions. In: *Fluid Inclusions in Minerals: Methods and Applications* (ed. by B. De Vivo & M.L. Frezzotti), I.M.A. Short Course, pp. 117–130. Virginia Polytechnic Institute and State University, USA.
- BOWERS, T.S. & HELGESON, H.C. (1983) Calculation of the thermodynamic and geochemical consequences of non ideal mixing in the system H_2O - CO_2 - NaCl on phase relations in geologic systems: Equation of state for H_2O - CO_2 - NaCl . *Geochim. Cosmochim. Acta*, **47**, 1247–1275.
- BROWN, P.E. & HAGGEMAN, S.G. (1995) Macflinclor: A computer program for fluid inclusion data reduction and manipulation. In: *Fluid Inclusions in Minerals: Methods and Applications* (ed. by B. De Vivo & M.L. Frezzotti), I.M.A. Short Course, pp. 231–250.
- BURRUS, R.C. (1989) Paleotemperatures from fluid inclusions: advances in theory and technique. In: *Thermal History of Sedimentary Basins. Methods and Case Histories* (ed. by N.D. Naeser & T.H. McCulloh), pp. 119–131. Springer-Verlag, New York.
- CAPOTE, R. (1983) La tectónica de la Cordillera Ibérica. In: *Geología de España. Libro Jubilar de J.M. Rios, Vol. 2* (ed. by J.A. Comba), pp. 108–120. ITGE, Madrid.
- CARTWRIGHT, I., POWER, W.L., OLIVER, N.H.S., VALENTA, R.K. & McLATCHIE, G.S. (1994) Fluid migration and vein formation during deformation and greenschist facies metamorphism at Ormiston Gorge, central Australia. *J. Metamorphic Geol.*, **12**, 373–386.
- CASAS, A.M., CORTÉS, A.L. & MAESTRO, A. (2000) Intra-plate deformation and basin formation in the northern Iberian plate: origin and evolution of the Almazán Basin. *Tectonics*, **19**, 258–289.
- CASAS-SAINZ, A.M. (1993) Oblique tectonic inversion and basement thrusting in the Cameros Massif (Northern Spain). *Geodinamica Acta*, **6**, 202–216.
- CASAS-SAINZ, A.M. & GIL-IMAZ A., (1998) Extensional subsidence, contractional folding and thrust inversion of the Eastern Cameros Massif, northern Spain. *Geol. Rdsch.*, **86**, 802–818.
- CASQUET, A., GALINDO, C., GONZÁLEZ-CASADO, J.M., ALONSO, A., MAS, R., RODAS, M., GARCÍA, E. & BARRENECHEA, J.F. (1992) El metamorfismo en la cuenca de los Cameros. Geocronología e implicaciones tectónicas. *Geogaceta*, **11**, 22–25.
- CLAYTON, R.N. & MAYEDA, T.K. (1963) The use of bromine pentafluoride in the extraction of oxygen from oxides and silicates for isotopic analysis. *Geochim. Cosmochim. Acta*, **27**, 43–52.
- CLAYTON, R.N., O'NEIL, J.R. & MAYEDA, T.K. (1972) Oxygen isotope exchange between quartz and water. *J. Geophys. Res.*, **77**, 3057–3067.
- DE CARITAT, P., HUTCHEON, I. & WALSH, J. (1993) Chlorite geothermometry: a review. *Clays Clay Minerals*, **41**, 219–239.
- DIÁZ-MARTÍNEZ, E. (1988) El Cretácico inferior del sector del Jubera (norte de la Sierra de Los Cameros, La Rioja): relación entre tectónica y sedimentación. *Procc. II Congreso Geológico España*, **1**, 67–70.
- DUNNE, W.M. & HANCOCK, P.L. (1994) Palaeostress analysis of small-scale brittle structures. In: *Continental Deformation* (ed. by P.L. Hancock), pp. 101–120. Pergamon Press, Oxford.
- ESSENE, E.J. & PEACOR, D.R. (1995) Clay mineral thermometry: a critical perspective. *Clays Clay Minerals*, **43**, 540–553.
- ESSENE, E.J. & PEACOR, D.R. (1997) Illite and smectite: metastable, stable, or unstable? Further discussion and a correction. *Clays Clay Minerals*, **45**, 116–122.

- ETHERIDGE, M.A., WALL, V.J. & VERNON, R.H. (1983) High fluid-pressures during regional metamorphism and deformation. *J. Metamorphic Geol.*, **1**, 205–226.
- FERREIRO, E., RUIZ, V., LENDÍNEZ, A., LAGO, M., MELÉNDEZ, A., PARDO, G., ARDEVOL, L., VILLENA, J., HERNÁNDEZ, A., ALVARO, M., GÓMEZ, J.J. & CARLS, P. (1991) *Mapa y memoria explicativa de la Hoja 40 (Daroca) del Mapa Geológico Nacional a escala 1:200.000*. ITGE, Madrid.
- FREY, M. (1987) Very low-grade metamorphism of clastic sedimentary rocks. In: *Low Temperature Metamorphism* (ed. by M. Frey). Blackie.
- GEHRIG, M. (1980) Phasengleichgewichte und pVT-Daten ternärer Mischungen aus Wasser, Kohlendioxid und Natriumchlorid bis 3 kbar und 500 °C. PhD Thesis, Karlsruhe., Hochschulsammlung Naturwissenschaft: Chemie; Bd. 1.
- GOLDBERG, J.M., GUIRAUD, M., MALUSKI, H. & SÉGURET, M. (1988) Caractères pétrologiques étage du métamorphisme en contexte distensif du bassin sur décrochement de Soria (Crétacé inférieur, Nord Espagne). *C. R. Acad. Sci. Paris*, **307**, 521–527.
- GOLDSTEIN, R.H. & REYNOLDS, T.J. (1994) *Systematics on Fluid Inclusions in Diagenetic Minerals*. Society for Sedimentary Geology Geology Short Course 31, S.E.P.M., Tulsa, OK.
- GOY, A., GÓMEZ, J.J. & YÉBENES, A. (1976) El Jurásico de la Rama Castellana de la Cordillera Ibérica (Mitad Norte). I. Unidades Litoestratigráficas. *Estudios Geológicos*, **32**, 391–423.
- GREEN, P.F., DUDDY, I.A. & BRAY, R.J. (1995) Applications of thermal history reconstruction in inverted basins. In: *Basin Inversion* (ed. by J.G. Buchanan & P.G. Buchanan), *Geol. Soc. Special Publication*, **88**, 149–165.
- GUIMERA, J., ALONSO, A. & MAS, J.R. (1995) Inversion of an extensional-ramp basin by a newly formed thrust: the Cameros basin (NSpain). In: *Basin Inversion* (ed. by J.G. Buchanan & P.G. Buchanan), *Geol. Soc. Special Publication*, **88**, 433–453.
- GUIMERA, J. & ALVARO, M. (1990) Structure et évolution de la compression alpine dans la Chaîne Ibérique et la Chaîne Cotière Catalane (Espagne). *Bull. Soc. Géol. France*, **8**, 339–348.
- GUIRAUD, M. (1983) Evolution tectono sédimentaire du bassin wealdien (Crétacé inférieur) en relais de décrochement de Logroño-Soria (NW Espagne). III cycle Thesis, University of Montpellier.
- GUIRAUD, M. & SÉGURET, M. (1984) Releasing solitary overstep model for the Late Jurassic-Early Cretaceous (Wealdien) Soria strike-slip basin (North Spain). In: *Strike-Slip Deformation, Basin Formation and Sedimentation* (ed. by K.T. Biddle & N. Cristhie-Blick), *SEPM Special Publication*, **37**, 159–175.
- HAGEN, E.S. & SURDAM, R.C. (1989) Thermal evolution of Laramide-Style Basins: Constraints from the Northern Bighorn Basin, Wyoming and Montana. In: *Thermal History of Sedimentary Basins: Methods and Case Histories* (ed. by N.D. Naeser & T. H. McCulloh), pp. 277–294. Springer-Verlag, New York.
- HANCOCK, P.L. (1985) Brittle microtectonics: principles and practice. *J. Struct. Geol.*, **7**, 437–457.
- HANOR, J.S. (1979) The sedimentary genesis of hydrothermal fluids. In: *Geochemistry of Hydrothermal Ore Deposits*, 2nd edn (ed. by H. Barnes). Wiley, New York.
- HEYDARI, E. (1997) Hydrotectonic models of burial diagenesis in platform carbonates based on formation water geochemistry in North American sedimentary basins. In: *Basin-Wide Diagenetic Patterns: Integrated Petrologic, Geochemical and Hydrologic Considerations*, *SEPM Special Publication*, **57**, 53–78.
- HOLLAND, T., POWELL, R. & WORLEY, B. (1998) Calculating phase diagrams involving solid solutions via non-linear equations, with examples using Thermocalc. *J. Metamorphic Geol.*, **16**, 577–588.
- JENSEN, R.P. & DORÉ, A.G. (1993) A recent Norwegian Shelf heating event—fact or fantasy?. In: *Basin Modelling: Advances and Applications* (ed. by A.G. Doré, et al.), Norwegian Petroleum Society Special Publication 3, pp. 85–106. Elsevier, Amsterdam.
- JUÁREZ, M.T., LOWRIE, W., OSETE, M.L. & MELÉNDEZ, G. (1998) Evidence of widespread Cretaceous remagnetisation in the Iberian Range and its relation with the rotation of Iberia. *Earth Planetary Sci. Lett.*, **160**, 729–743.
- JUÁREZ, M.T., OSETE, M.L., MELÉNDEZ, G., LANGEREIS, C.G. & ZIJDERVELD, J.D.A. (1994) Oxfordian magnetostratigraphy of the Aguilón and Tosos sections (Iberian Range, Spain) and evidence of a pre-Oligocene overprint. *Physics Earth Planetary Interiors*, **85**, 195–211.
- JULIVERT, M. (1978) The areas of Alpine folded cover in the Iberian Meseta (Iberian Chain, Catalanides, etc.). In: *Geological Atlas of Alpine Europe and Adjoining Alpine Areas*, pp. 93–112. Elsevier, New York.
- KIRSCHNER, D.L., SHARP, Z.D. & MASSON, H. (1995) Oxygen isotope thermometry of quartz-calcite veins: Unraveling the thermal-tectonic history of the subgreenschist facies Morcles nappe (Swiss Alps). *Geol. Soc. Am. Bull.*, **107**, 1145–1156.
- LAGO, M., POCIVI, A., BASTIDA, J. & AMIGÓ, J.M. (1988) The alkaline magmatism in the Triassic-Liassic boundary of the Iberian Chain: geological and petrological characters. *II Congreso Geológico España, Granada, Comunicaciones*, **2**, 31–34.
- LANAJA, J.M. (1987) *Contribución de la Exploración Petrolífera Al Conocimiento de la Geología de España*. Instituto Geológico y Minero de España, Madrid.
- LERCHE, I. (1993) Theoretical aspects of problems in basin modelling. In: *Basin Modelling: Advances and Applications* (ed. by A.G. Doré, et al.), Norwegian Petroleum Society Special Publication 3, pp. 35–65. Elsevier, Amsterdam.
- MAGARA, K. (1976) Thickness of removed sedimentary rocks, paleopressure and paleotemperature, southwestern part of Western Canada Basin. *AAPG Bull.*, **60**, 554–565.
- MAS, J.R., ALONSO, A. & GUIMERA, J. (1993) Evolución tectono sedimentaria de una cuenca extensional intraplaca: la cuenca finijurásica-eocretácica de Los Cameros (La Rioja-Soria). *Rev. Soc. Geol. Esp.*, **6**, 129–144.
- MATA CAMPO, M.P. (1997) *Caracterización y evolución mineralógica de la Cuenca mesozoica de Cameros (Soria – La Rioja)*. PhD Thesis, University of Zaragoza.
- MATA CAMPO, M.P., GIL-IMAZ, A., CASAS-SAINZ, A., POCIVI JUAN, A. & CANALS, A. (1996) La extensión cretácica en la Cuenca de Cameros: resultados del análisis estructural de grietas de cuarzo y del estudio de inclusiones fluidas. *Geogaceta*, **20**, 893–896.
- MATA CAMPO, M.P., LÓPEZ-AGUAYO, F. & PEACOR, D.R. (1998) Evidence for a low-P–T origin of cookeite polytypes in pelites of the Iberian Range (Spain): a TEM study. *17th*

- Meeting of the International Mineralogical Association*. International Mineralogical Association, Toronto, Canada.
- MATA, M.P., OSACAR, M.C. & LÓPEZ-AGUAYO, F. (2000) Una aproximación al área fuente del Weald de Cameros: Datos geoquímicos. *Geotemas*, **1**, (3) 263–265.
- MCDONALD, A.E., VON ROSENBERG, D.U., JINES, W.R., BURKE, W.H. & UHLER, L.M. (1989) A simulator for the computation of paleotemperatures during basin evolution. In: *Thermal History of Sedimentary Basins: Methods and Case Histories* (ed. by N.D. Naeser & T.H. McCulloh), pp. 277–294. Springer-Verlag, Berlin.
- MCKENZIE, D.P. (1978) Some remarks on the development of sedimentary basins. *Earth Planetary Sci. Lett.*, **40**, 25–32.
- MCREA, J.M. (1950) On the isotopic chemistry of carbonates and a paleotemperature scale. *J. Chem. Phys.*, **18**, 849–857.
- MERRIMAN, R.J. & FREY, M. (1999) Patterns of very low-grade metamorphism in metapelitic rocks. In: *Low-Grade Metamorphism* (ed. by M. Frey & D. Robinson), pp. 61–108. Blackwell Science, Oxford.
- MERRIMAN, R.J. & PEACOR, D.R. (1999) Very low-grade metapelites: mineralogy, microfabrics and measuring reaction progress. In: *Low-Grade Metamorphism* (ed. by M. Frey & D. Robinson), pp. 10–61. Blackwell Science, Oxford.
- MIALL, A.D. (1984) *Principles of Sedimentary Basin Analysis*. Springer-Verlag, Berlin.
- MULLIS, J. (1987) Fluid inclusions studies during very low-grade metamorphism. In: *Low Temperature Metamorphism* (ed. by M. Frey). Blackie, Glasgow.
- MUÑOZ, A., SORIA, A.R., CANUDO, J.I., CASAS, A.M., GIL, A. & MATA, M.P. (1997) Caracterización estratigráfica y sedimentológica del Albiense marino del borde Norte de la Sierra de Cameros. Implicaciones paleogeográficas. *Cuad. Geol. Ibérica*, **22**, 139–163.
- MUÑOZ-JIMÉNEZ, A. & CASAS-SAINZ, A.M. (1996) The Rioja Trough (NSpain): tecto-sedimentary evolution of a symmetric foreland basin. *Basin Res.*, **9**, 65–85.
- MUÑOZ-MARTÍN, A. & DE VICENTE, G. (1998) Cuantificación del acortamiento alpino y estructura en profundidad del extremo suroccidental de la Cordillera Ibérica (Sierras de Altomira y Bascuñana). *Rev. Soc. Geol. Esp.*, **11**, 233–252.
- NAESER, N.D., NAESER, C.W. & MCCULLOH, T.H. (1989) The application of fission-track dating to the depositional and thermal history of rocks in sedimentary basins. In: *Thermal History of Sedimentary Basins. Methods and Case Histories* (ed. by N.D. Naeser & T.H. McCulloh), pp. 157–180. Springer Verlag, Berlin.
- OLIVER, J. (1986) Fluids expelled tectonically from orogenic belts: Their role in hydrocarbon migration and other geologic phenomena. *Geology*, **14**, 99–102.
- PLATT, N.H. (1990) Basin evolution and fault reactivation in the Western Cameros Basin, Northern Spain. *J. Geol. Soc. London*, **147**, 165–175.
- POCOVI, A., MELÉNDEZ, A. & MELÉNDEZ, G. (1997) Los aspectos más obvios del Jurásico de los Pirineos. *Comunicaciones IV Congreso de Jurásico de España*, Alcañiz, 17–19.
- QUIGLEY, T.M. & MCKENZIE, A.S. (1988) The temperatures of oil and gas formation in the sub-surface. *Nature*, **333**, 549–552.
- RAMSAY, J.G. & HUBER, M.I. (1983) *The Techniques of Modern Structural Geology, 1, Strain Analysis*. Academic Press, London.
- ROYDEN, L., SCLATER, J.G. & HERZEN, P.V. (1980) Continental margin subsidence and heat flow: important parameters in formation of petroleum hydrocarbons. *A.A.P.G. Bull.*, **64**, 173–187.
- SALAS, R. & CASAS, A. (1993) Mesozoic extensional tectonics, stratigraphy and crustal evolution during the Alpine cycle of the eastern Iberian basin. *Tectonophysics*, **228**, 33–35.
- SALOMON, J. (1980) Apparition des principales traits structuraux de la Sierra de Los Cameros (Chaîne Ibérique, Espagne du Nord) au Jurassique supérieur-Crétacé inférieur. *C. R. Acad. Sci. Paris*, **290**, 955–958.
- SHARP, Z.D. (1999) Application of stable isotope geochemistry to low-grade metamorphic rocks. In: *Low-Grade Metamorphism* (ed. by M. Frey & D. Robinson), pp. 227–259. Blackwell Science, Oxford.
- SHARP, Z.D. & KIRCHNER, D.L. (1994) Quartz calcite oxygen isotope thermometry; a calibration based on natural isotopic variations. *Geochim. Cosmochim. Acta*, **58**, 4491–4501.
- SOPEÑA, A., VIRGILI, C., ARCHE, A., RAMOS, A. & HERNANDO, S. (1983) El Triásico. In: *Geología de España, Libro Jubilar J.M. Ríos*, 2 (ed. by J.A. Comba), pp. 47–63. Instituto Geológico y Minero de España.
- TER VOORDE, M. & BERTOTTI, G. (1994) Thermal effects of normal faulting during rifted basin formation, 1. A finite difference model. *Tectonophysics*, **240**, 133–144.
- TISCHER, G. (1966) El delta Wealdico de las montañas Ibéricas Occidentales y sus enlaces tectónicos. *Notas Y Comunicaciones Instituto Geológico Y Minero España*, **81**, 53–78.
- WALL, V.J. & ETHERIDGE, M.A. (1988) Regional metamorphic fluid migration: single pass or circulation?. *E.O.S.*, **69**, 464.
- WILLETT, S.D., ISSLER, D.R., BEAUMONT, C., DONELICK, R.A. & GRIST, A.M. (1997) Inverse modelling of annealing of fission tracks in apatite: application to the thermal history of the Peace River Arch. region, Western Canada sedimentary basin. *Am. J. Sci.*, **297**, 970–1011.
- YARDLEY, B.W.D. & BOTRELL, S.H. (1992) Silica mobility and fluid movement during metamorphism of the Connemara schists, Ireland. *J. Metamorphic Geol.*, **10**, 453–464.
- ZHAO, M.-W., BEHR, H.-J., AHRENDT, H., WEMMER, K., REN, Z.-L. & ZHAO, Z.-Y. (1996) Thermal and tectonic history of the Ordos Basin, China: evidence from apatite fission track analysis, vitrinite reflectance and K–Ar dating. *AAPG Bull.*, **80**, 1110–1134.
- ZIEGLER, P.A. (1989) Geodynamic model for Alpine intra-plate compressional deformation in Western and Central Europe. In: *Inversion Tectonics* (ed. by M.A. Cooper & G.D. Williams), *Geol. Soc. Spec. Publ.*, **44**, 63–85.

Received 6 January 2000; revision accepted 12 September 2000